Title: The Role of Intercalated Cell lt;igt;Nedd4-2lt;/igt; in BP Regulation, Ion Transport, and Transporter Expression.

Authors: Nanami M, Pham TD, Kim YH, Yang B, Sutliff RL, Staub O, Klein JD, Lopez-Cayuqueo KI, Chambrey R, Park AY, Wang X, Pech V, Verlander JW, Wall SM

Journal: Journal of the American Society of Nephrology : JASN

Year: 2018 Jun

Issue: 29

Volume: 6

Pages: 1706-1719

DOI: 10.1681/ASN.2017080826

The Role of Intercalated Cell *Nedd4-2* in BP Regulation, Ion Transport, and Transporter Expression

Running title: Intercalated Cell *Nedd4-2*

Masayoshi Nanami[1*], Truyen D. Pham[1*], Young Hee Kim[1], Baoli Yang[2], Roy L. Sutliff[3], Olivier Staub[4,5], Janet D. Klein[1], Karen I. Lopez-Cayuqueo[6,7], Regine Chambrey[8], Annie Y. Park[1], Xiaonan Wang[1], Vladimir Pech[1], Jill W. Verlander[9t] and Susan M. Wall[1,10t]

*These authors contributed equally

[t]These authors contributed equally

[1] Renal and [3]Pulmonary Divisions in the Department of Medicine and [10]Department of Physiology, Emory University School of Medicine, Atlanta, GA
[2]Department of Obstetrics and Gynecology, University of Iowa, Iowa City, IA
[4]Department of Pharmacology and Toxicology, University of Lausanne, Lausanne, Switzerland
[5]National Centre of Competence in Research "Kidney.ch", Switzerland
[6]Centro de Estudios Cientificos (CECs), Valdivia, Chile
[7]INSERM U970, Paris Cardiovascular Research center, Université Paris-Descartes, Paris, France
[8]INSERM U1188; Universite de la Reunion; Plateforme CYROI, F97400, St. Denis, Ile de la Reunion, France
[9]Renal Division, Department of Medicine, University of Florida at Gainesville, Gainesville, FL

Correspondence:

Susan M. Wall, M.D.
Renal Division
Emory University School of Medicine
WMB Rm. 338, 1639 Pierce Dr., NE
Atlanta, GA 30322
Phone: (404) 727-2525
FAX: (404) 727-3425
e-mail: smwall@emory.edu

ABSTRACT:

BACKGROUND: The E3 ubiquitin-protein ligase encoded by *Nedd4-2* associates with transport proteins, causing the ubiquitylation and subsequent internalization and degradation thereof. Previous research has suggested a correlation between *Nedd4-2* and BP. In this study, we explored the effect of intercalated cell (IC) *Nedd4-2* gene ablation on IC transporter abundance and function and on BP.

METHODS: We generated IC *Nedd4-2*-knockout mice using Cre-lox technology and produced global pendrin/*Nedd4-2*-null mice by breeding global *Nedd4-2*-null (*Nedd4-2*$^{-/-}$) mice with global pendrin-null (*Slc26a4*$^{-/-}$) mice. Mice ate a diet with 1%–4% NaCl; BP was measured by tailcuff and radiotelemetry. We measured transepithelial transport of Cl^- and total CO_2 and transepithelial voltage in cortical collecting ducts perfused *in vitro*. Transporter abundance was detected with immunoblots, immunohistochemistry, and immunogold cytochemistry.

RESULTS: IC *Nedd4-2* gene ablation markedly increased electroneutral Cl^-/HCO_3^- exchange in the cortical collecting duct, although benzamil-, thiazide-, and bafilomycin-sensitive ion flux changed very little. IC *Nedd4-2* gene ablation did not increase the abundance of type B IC transporters, including AE4 (*Slc4a9*), H^+-ATPase, barttin, or the Na^+-dependent Cl^-/HCO_3^- exchanger (*Slc4a8*). However, IC *Nedd4-2* gene ablation increased the total protein abundance of H^+/Cl^- exchange transporter 5, the apical membrane abundance of pendrin, and the ratio of pendrin expression on the apical membrane to that in the cytoplasm. IC *Nedd4-2* gene ablation increased BP by approximately 10 mmHg. Moreover, pendrin gene ablation eliminated the increase in BP observed in global *Nedd4-2*-knockout mice.

CONCLUSION: IC *Nedd4-2* regulates Cl^-/HCO_3^- exchange in ICs, and *Nedd4-2* gene ablation increases BP in part through actions in these cells.

INTRODUCTION:

In people and in rodent models of salt-sensitive hypertension, blood pressure elevation requires increased intake of Na^+ and Cl^- (21, 22). One commonly used rodent model of human salt sensitive hypertension is achieved with the administration of aldosterone and a high NaCl diet. This treatment model produces salt-sensitive hypertension partly by stimulating renal Na^+ and Cl^- transporters such as the epithelial Na^+ channel, ENaC (25), the thiazide-sensitive NaCl cotransporter, NCC (17), and pendrin (52). Aldosterone modulates NaCl absorption, at least in some renal cell types, by changing the number of functional transporters in the cell membrane partly through a mechanism that involves the E3 ubiquitin-protein ligase, neuronal precursor cell expressed developmentally downregulated (*Nedd4-2)* (2, 7, 47) (11). When a transporter or a channel associates with *Nedd4-2*, it is ubiquitylated and then endocytosed and degraded in proteasomes or lysosomes (11, 24, 41). Conversely, in the absence of *Nedd4-2*, i.e. in *Nedd4-2* knockout mice, channel internalization and degradation fall, which increases ENaC plasma membrane abundance, thereby contributing to the salt-sensitive hypertension observed in global *Nedd4-2* null mice (47). As such, increased blood pressure is observed in mice with embryonic, global *Nedd4-2* gene ablation (47), in mice with inducible, kidney-specific *Nedd4-2* gene ablation (40) and in people with certain polymorphisms of *NEDD4-L*, the human homologue of rodent *Nedd4-2* (16, 61).

The Na^+ and Cl^- transporters expressed in principal cells and in the various intercalated cell subtypes are displayed in Figure 1. In the cortical collecting duct (CCD), Na^+ is absorbed primarily by principal cells, whereas Cl^- is absorbed primarily across intercalated cells (44), largely through electroneutral Cl^-/HCO_3^- exchange across type B intercalated cells (49). Apical anion exchange occurs through apical Na^+-independent Cl^-/HCO_3^- exchange, mediated

principally by pendrin (*Slc26a4*) (42, 59), which acts in parallel with the Na^+-dependent Cl^-/HCO_3^- exchanger, NDCBE, encoded by *Slc4a8* (23)(Figure 1). NaCl and net H^+ equivalents exit across the type B intercalated cell basolateral plasma membrane through a Cl^- channel (ClC-K2/barttin or ClC-Kb) (13, 36), a $NaHCO_3$ cotransporter (AE4) (5) and a H^+ pump (H^+-ATPase) (5) (Figure 1). This NaCl and H^+ exit increases the electrochemical gradient for apical anion exchange, thereby increasing Cl^- absorption and HCO_3^- secretion. In contrast to type B intercalated cells, type A intercalated cells mediate net HCl secretion into the luminal fluid (29, 30, 56, 57) in series with Cl^- uptake and HCO_3^- exit across the basolateral membrane through Cl^-/HCO_3^- exchange (AE1), a Na^+-K^+-2Cl^- cotransporter (NKCC1) and a Cl^- channel (Figure 1) (13, 33, 36, 57).

Nedd4-2 is expressed in the aldosterone-sensitive region of the nephron (24), which includes the CNT, the CCD and the OMCD. Mouse connecting tubule (CNT) is made up of CNT cells and intercalated cells, whereas mouse CCD is composed of principal cells and intercalated cells (58). *Nedd4-2* is highly expressed in the CCD and CNT (24), particularly within type B and Non-A, non-B intercalated cells, CNT cells and principal cells, with much lower abundance in type A intercalated cells (24). While the role of *Nedd4-2* in principal cells has been well studied, little is known about its function in intercalated cells. Our ability to generate mice in which *Nedd4-2* gene ablation has occurred specifically within intercalated cells of the CCD plus our ability to perfuse CCDs in vitro from these mice (60) provide a unique opportunity by which to explore the physiological role of IC *Nedd4-2* in native tissue.

Aldosterone's signal transduction mechanism in type B intercalated cells is poorly understood. Because *Nedd4-2* participates in aldosterone signaling in many cell types and because *Nedd4-2* is expressed in intercalated cells, we sought to determine if *Nedd4-2* changes

blood pressure by altering intercalated cell function. The purpose of this study was to determine if IC *Nedd4-2* gene ablation changes CCD ion transport or blood pressure and to determine the transporter(s) regulated by *Nedd4-2* within intercalated cells.

METHODS:

Animals: Intercalated cell (IC) *Nedd4-2* null mice were generated by breeding floxed *Nedd4-2* mice (47) with transgenic mice expressing Cre recombinase driven by the ATP6V1B1 promoter (B1-H^+-ATPase Cre) (26), a subunit of the H^+-ATPase that is expressed in renal intercalated cells (26). The Cre was bred through the female line. We compared IC *Nedd4-2* null (*Nedd4-2*^{loxloxcre}) with Cre (-), gender-matched, wild type littermates (*Nedd4-2*^{loxlox}). Unless otherwise stated, IC *Nedd4-2* KO and wild type littermates will refer to *Nedd4-2*^{loxloxcre} and *Nedd4-2*^{loxlox}, respectively. Mice were genotyped by quantitative PCR (Transnetyx) and sometimes by standard PCR (26, 47).

Global *Nedd4-2* null mice were generated as described previously (47), by breeding floxed *Nedd4-2* mice with mice expressing Cre recombinase globally (EIIa-Cre, Jackson Labs, Stock # 003724) (47). To generate *Nedd4-2*$^{-/-}$/*Slc26a4*$^{-/-}$; *Nedd4-2*$^{+/+}$/*Slc26a4*$^{-/-}$, *Nedd4-2*$^{-/-}$/*Slc26a4*$^{+/+}$ and wild type littermates on a C57Bl/6 background, we first bred global pendrin null (*Slc26a4*$^{-/-}$) on a 129 SvEv Tac background with wild type mice on a C57Bl/6 background over 10 generations. We then bred global *Nedd4-2* null (*Nedd4-2*$^{-/-}$) and pendrin null mice (*Slc26a4*$^{-/-}$), both on a C57Bl/6 background, to generate *Nedd4-2*$^{-/-}$/*Slc26a4*$^{-/-}$; *Nedd4-2*$^{+/+}$/*Slc26a4*$^{-/-}$, *Nedd4-2*$^{-/-}$/*Slc26a4*$^{+/+}$ and wild type mice, which were all Cre$^{-/-}$.

Unless otherwise indicated, mice ate a balanced diet (53881300; Zeigler Brothers) prepared as a gel (0.6% agar, 74.6% water, and 24.8% mouse chow) supplemented with NaCl, which provided each mouse ~ 1.4 mEq NaCl per day (~2% NaCl), which they ate for 5-7 days before sacrifice. In blood pressure studies, mice ate a diet with 1% (LabDiet5001) or 4% NaCl (Teklad TD92034) and drank water ad libitum for 7 to 14 days prior to study.

Statistics: Results are expressed as the mean ± S.E. The "n" represents the number of mice studied.

All other methods are given in the SUPPLEMENTAL METHODS section.

RESULTS:

IC Nedd4-2 is reduced in B1 H^+-ATPase Cre; Nedd4-2^{loxloxcre} mice.

To explore the impact of *Nedd4-2* on intercalated cell function, we generated IC *Nedd4-2* null mice using Cre-lox technology (B1-ATPase Cre; *Nedd4-2*^{loxloxcre}). To determine if *Nedd4-2* knockdown is restricted to intercalated cells, we examined Cre recombinase localization in these mice by breeding them with Cre reporter mice (tdTomato mice) and studying their offspring. In cells expressing Cre recombinase, a stop codon is deleted, resulting in tdTomato expression, which fluoresces red (28). Intercalated cells were identified by combined AE1 and pendrin labeling (4). Figure 2A shows dTomato (Cre recombinase, red) expression in the majority of pendrin/AE1 positive cells (intercalated cells, green) of the CCD, with only occasional expression in pendrin/AE1 negative cells (principal cells). In the CNT, dTomato labeling was also observed in the majority of pendrin/AE1 positive cells (intercalated cells), although about 50% of CNT cells had weak dTomato labeling, consistent with previous reports (26, 27). dTomato labeling was also observed in occasional glomeruli, occasional blood vessels and in some cells within the interstititium (Figures 2B & C).

To evaluate the specificity of IC *Nedd4-2* gene ablation further, we examined *Nedd4-2* labeling (brown) in CCDs taken from IC *Nedd4-2* knockout and in wild type littermates (Figure 3). AQP2 (dark blue) label identified principal cells. The distribution of *Nedd4-2* positive and negative cells was quantified in CCDs from mice in each group (Table 1). As shown, nearly all AQP2 positive cells (principal cells) labeled for *Nedd4-2*, whether taken from the IC *Nedd4-2* null or their wild type littermates (floxed *Nedd4-2*). *Nedd4-2* label was absent in 28% of intercalated cells from wild type CCDs, which is consistent with previous reports showing weak *Nedd4-2* expression in mouse type A intercalated cells (24). However, *Nedd4-2* immunolabel

was absent in 72% of intercalated cells from IC *Nedd4-2* null CCDs. Because these experiments show significant *Nedd4-2* knockdown in intercalated cells of CCDs from IC *Nedd4-2* null mice, with little knockdown in principal cells, and because mouse CCD can be perfused in vitro, this study focused primarily on the effect of IC *Nedd4-2* gene ablation on ion transport in mouse CCD.

Nedd4-2 gene ablation in principal cells increases apical plasma membrane ENaC abundance, which stimulates Na^+ absorption, thereby increasing the lumen-negative transepithelial voltage (Figure 1) (47). With increased ENaC-mediated Na^+ absorption, a greater fall in the lumen-negative V_T is observed with the application of ENaC inhibitors, such as benzamil, which thereby increases benzamil-sensitive transepithelial voltage, V_T. To determine if *Nedd4-2* gene ablation has occurred within principal cells, we compared ENaC activity in CCDs from global *Nedd4-2* null, IC *Nedd4-2* null and their wild type controls by measuring benzamil-sensitive V_T in CCDs from mice in each group. Figure 4 shows significant benzamil-sensitive V_T in CCDs from global *Nedd4-2* KO mice where *Nedd4-2* gene ablation has occurred in both intercalated cells and principal cells (47). In contrast, benzamil-sensitive V_T was low in the IC *Nedd4-2* null CCDs and not significantly different from that measured in their wild type littermates (Figure 4). These data show little increase in ENaC activity in principal cells of CCDs from IC *Nedd4-2* KO mice, which is consistent with minimal *Nedd4-2* knockdown in this cell type.

IC Nedd4-2 gene ablation does not change serum electrolytes, aldosterone or arterial pH

Since intercalated cell transporters are frequently modulated by changes in serum aldosterone concentration, acid-base balance or serum electrolytes, we examined each of these in

IC *Nedd4-2* KO and wild type littermates. Table 2 shows that serum electrolytes and arterial blood gases are similar in both groups of mice. Since serum aldosterone is the same or lower in the IC *Nedd4-2* null relative to wild type littermates, if *Nedd4-2* gene ablation increases the abundance or function of an intercalated cell transporter, it does not do so through increased circulating aldosterone.

IC Nedd4-2 gene ablation increases electroneutral Cl^-/HCO_3^- exchange in mouse CCD.

Since intercalated cells mediate Cl^- and HCO_3^- transport, we examined the effect of IC *Nedd4-2* gene ablation on transepithelial Cl^- and HCO_3^- transport. Figure 5A shows Cl^- secretion and HCO_3^- absorption in CCDs taken from wild type mice consuming the high NaCl diet, similar to our previous observations (29, 32). In contrast, CCDs from IC *Nedd4-2* null mice absorb, rather than secrete, Cl^- and secrete, rather than absorb, HCO_3^-. Transepithelial voltage was low and not statistically different in CCDs from IC *Nedd4-2* KO and their wild type littermates (Figure 5A). Therefore, IC *Nedd4-2* gene ablation increases electroneutral Cl^-/HCO_3^- exchange in mouse CCD.

ENaC is a *Nedd4-2*-regulated channel that provides the driving force for the benzamil-sensitive Cl^- absorption in mouse CCD, which may occur through paracellular Cl^- transport (29, 33). Therefore, we asked if Cl^- absorption is higher in CCDs from global *Nedd4-2* null mice, where *Nedd4-2* gene ablation has occurred in both principal and in intercalated cells, than in IC *Nedd4-2* KO mice, where *Nedd4-2* gene ablation has been restricted to intercalated cells. Figure 5B shows, however, that global *Nedd4-2* deletion resulted in changes in Cl^- flux that were numerically and directionally similar to those observed in the IC *Nedd4-2* null mice. We

conclude that the change in CCD Cl^- transport that follows global *Nedd4-2* gene ablation is predominantly transcellular through intercalated cells.

IC Nedd4-2 gene ablation produces only a small increment in net H^+ flux, J_{tCO2}, that is sensitive to H^+-ATPase inhibitors.

While pendrin is thought to mediate the 1:1 exchange of Cl^- and HCO_3^- (46), IC *Nedd4-2* gene ablation increased Cl^- absorption more than HCO_3^- secretion. We therefore asked if IC *Nedd4-2* gene ablation increases apical H^+-ATPase abundance and function, thereby attenuating the increment in luminal HCO_3^- concentration generated with increased apical Cl^-/HCO_3^- exchange. If so, inhibiting H^+ secretion by the type A intercalated cell should increase HCO_3^- secretion more in CCDs from the IC *Nedd4-2* KO than their wild type littermates. To address this question, we measured J_{tCO2} before and after the application of an H^+-ATPase inhibitor (bafilomycin) to the luminal fluid. Supplemental Figure 1A shows that apical H^+-ATPase blockade produced a small increment in tCO2 secretion in the intercalalated cell *Nedd4-2* KO mice, but not in the wild type littermates. However, H^+-ATPase abundance and subcellular distribution in type A intercalated cells were similar in kidneys from IC *Nedd4-2* null and wild type littermates (Supplemental Figure 1B and Supplemental Table 1). We conclude that while *Nedd4-2* gene ablation increases H^+ secretion by type A intercalated cells, this change is small and is not accompanied by an increment in H^+-ATPase protein abundance in the apical region. The absence of an effect of *Nedd4-2* gene ablation on H^+-ATPase abundance and function in type A intercalated cells is either because *Nedd4-2* expression is low in type A intercalated cells or because the apical H^+-ATPase is not significantly modulated by *Nedd4-2*.

IC Nedd4-2 gene ablation produces little change in either thiazide- or benzamil-sensitive Cl^- absorption and does not increase thiazide-sensitive exchanger, NDCBE, abundance

In the rodent CCD, Cl^- absorption occurs through thiazide- and amiloride (benzamil)-sensitive mechanisms (51). The former occurs through electroneutral NaCl absorption that involves the Na^+-dependent Cl^-/HCO_3^- exchanger, NDCBE, encoded by *Slc4a8* (23), while the latter occurs through an electrogenic mechanism driven by the lumen-negative voltage generated by ENaC-mediated Na^+ absorption (29).

To determine if IC *Nedd4-2* gene ablation increases NDCBE-mediated Cl^- absorption, we compared thiazide-sensitive Cl^- absorption in CCDs from IC *Nedd4-2* null and wild type littermates. Figure 6A shows that Cl^- absorption fell slightly with the application of hydrochlorothiazide (HCTZ) to the perfusate in CCDs from the IC *Nedd4-2* null, but not from wild type littermates, suggesting that IC *Nedd4-2* gene ablation stimulates NDCBE-mediated NaCl absorption. However, while Cl^- absorption was ~23 pmol/mm/min higher in CCDs from IC *Nedd4-2* KO than wild type littermates, thiazide-sensitive Cl^- absorption rose by only ~1.5 pmol/mm/min (Figure 6B). As such, the increment in thiazide-sensitive Cl^- absorption observed with IC *Nedd4-2* gene ablation is relatively small.

Because IC *Nedd4-2* gene ablation produced a small increment in the thiazide-sensitive component of Cl^- absorption, further experiments examined the effect of IC *Nedd4-2* gene ablation on NDCBE (*Slc4a8*) total protein abundance in kidney lysates from IC *Nedd4-2* null and wild type littermates. Figure 6C shows that NDCBE band intensity was no higher in kidney lysates from IC *Nedd4-2* null than in wild type mice. We could not examine the effect of IC *Nedd4-2* gene ablation on NDCBE subcellular distribution due to the absence of an antibody

suitable for immunohistochemistry or immunogold cytochemistry. We conclude that IC *Nedd4-2* gene ablation does not produce a marked change in NDCBE abundance or function.

Further experiments examined the effect of IC *Nedd4-2* gene ablation on the benzamil-sensitive component of Cl^- absorption, J_{Cl} (Figure 7). As shown, benzamil-sensitive J_{Cl} was similar in CCDs from Cre (+), IC *Nedd4-2* KO and Cre (-), wild type littermates. We conclude that the benzamil-sensitive component of J_{Cl} is unaffected by IC *Nedd4-2* gene ablation.

Nedd4-2 gene ablation increases ClC-5 abundance in type B but not in type A intercalated cells.

Because ClC-5 gene ablation might modulate Cl^- absorption in the CCD of aldosterone-treated mice (29), we used quantitative immunohistochemistry to explore the effect of global *Nedd4-2* gene ablation on ClC-5 abundance and subcellular distribution. Total ClC-5 label and ClC-5 label in the most apical 20% of the cell was quantified in type A and type B intercalated cells from CCDs of global *Nedd4-2* null and wild type littermates. Figure 8A shows ClC-5 label in AE1 (+) type A and AE1 (-) type B intercalated cells. Figures 8B & C show that in type A intercalated cells, ClC-5 label intensity per cell as well as ClC-5 label intensity in most apical 20% of the cell were similar in IC *Nedd4-2* null and in wild type littermates. In type B intercalated cells, however, total label per cell and label in the most apical 20% of the cell were higher in the IC *Nedd4-2* null mice (figures 8D & E). We conclude that while *Nedd4-2* does not alter ClC-5 abundance or subcellular distribution in type A intercalated cells, *Nedd4-2* gene ablation increases ClC-5 total protein abundance and the relative abundance of ClC-5 in the region of the apical plasma membrane of type B intercalated cells.

IC Nedd4-2 gene ablation increases pendrin abundance in the apical plasma membrane region

Since IC *Nedd4-2* gene ablation increases apical anion exchange and since electroneutral apical anion exchange in the CCD is largely pendrin-dependent, further experiments explored the effect of *Nedd4-2* gene ablation on total and apical plasma membrane pendrin protein abundance and pendrin subcellular distribution. We observed that pendrin immunolabel is slightly more prominent in kidney sections from the IC *Nedd4-2* null than in wild type littermates (Figure 9A-F). Figures 9G-I show that IC*Nedd4-2* gene ablation either produced no change or slightly increased pendrin total protein abundance. In contrast, Figure 9J shows that pendrin mRNA was either unchanged or reduced with IC *Nedd4-2* gene ablation.

Further experiments examined the effect of IC *Nedd4-2* gene ablation on apical plasma membrane and cytoplasm pendrin abundance. Immunogold cytochemistry with morphometric analysis was used to quantify pendrin total protein abundance and pendrin subcellular distribution in both type B and Non-A, non-B intercalated cells of mice from each group. Supplemental Figure 2 shows pendrin gold label in a typical type B intercalated cell taken from both an IC *Nedd4-2* null mouse and a wild type littermate. Table 3 shows apical plasma membrane and cytoplasm pendrin gold in both type B and Non-A, non-B intercalated cells from IC *Nedd4-2* null and wild type littermates. As shown, apical plasma membrane pendrin immunogold per type B intercalated cell was the same or slightly higher in IC *Nedd4-2* KO relative to their wild type littermates. However, type B intercalated cell apical plasma membrane boundary length was 42% higher and the ratio of apical plasma membrane to cytoplasm pendrin abundance more than 2-fold higher in the IC *Nedd4-2* null relative to their wild type littermates.

In Non-A, non-B intercalated cells, the predominant pendrin positive cell type in the CNT, IC *Nedd4-2* gene ablation increased apical plasma membrane boundary length 48% and increased apical plasma membrane pendrin (gold) label per cell by 80% (Table 3). However, differences in the ratio of pendrin (gold) label on the apical plasma membrane relative to subapical vesicles in this cell type did not reach statistical significance. These data show that IC *Nedd4-2* gene ablation increases apical plasma membrane pendrin abundance in the Non-A, non-B intercalated cell.

Intercalated cell Nedd4-2 gene ablation does not increase AE4, H^+-ATPase or barttin abundance

Nedd4-2 gene ablation may increase apical Cl^-/HCO_3^- exchange by interacting with a basolateral plasma membrane transporter in type B intercalated cells (Figure 1), which increases the driving force for apical anion exchange by enhancing Na^+, Cl^- and H^+ exit. To test this hypothesis, we examined the effect of intercalated cell *Nedd4-2* gene ablation on the abundance and subcellular distribution of the type B intercalated cell transporters that localize to the basolateral membrane and mediate this Na^+, Cl^- or H^+ exit (Figure 1). As shown (Supplemental Figures 3 & 4), IC *Nedd4-2* gene ablation did not increase AE4 or barttin total immunolabel intensity or label intensity in the region of the plasma membrane. Moreover, using immunogold cytochemistry we observed that basolateral plasma membrane barttin gold label was not increased in type B intercalated cells from IC *Nedd4-2* null relative to wild type littermates (not shown).

Because the basolateral H^+-ATPase provides the driving force for apical anion exchange (5), we examined total α4 H^+-ATPase immunolabel and α4 H^+-ATPase subcellular distribution

in type B intercalated cells from IC *Nedd4-2* null and wild type littermates (Supplemental Figure 1 and Supplemental Table 1). No difference in type B intercalated cell H^+-ATPase abundance or subcellular distribution was detected by quantitative analysis of H^+-ATPase α4 subunit immunolabel in mice from these two groups.

These data show that while AE4, H^+-ATPase or ClC-K2/bartin modulate apical anion exchange in mouse CCD, it does not likely occur through an interaction with *Nedd4-2*.

IC Nedd4-2 modulates blood pressure.

To explore the role of *Nedd4-2* within intercalated cells on blood pressure regulation, we examined the effect of IC *Nedd4-2* gene ablation on blood pressure. By tailcuff, we observed systolic blood pressure to be similar in IC *Nedd4-2* KO in wild type littermates following a standard rodent diet (1% NaCl, Supplemental Figure 5). However, after 14 days of a 4% NaCl diet, which increases *Nedd4-2* expression in wild type mice (24), systolic blood pressure was higher in the IC *Nedd4-2* KO than in the wild type littermates. To confirm these findings, 24 hour blood pressure recordings were made using radiotelemetry after mice were given 7 days of a high NaCl (4% NaCl) diet. Over a 24 hour period, mean arterial pressure was 107 ± 1.1 (n=4) in the IC *Nedd4-2* null and 97 ± 0.9 mm Hg (n=5) in the wild type littermates ($P < 0.05$). Therefore, blood pressure was ~10 mm Hg higher in the IC *Nedd4-2* KO than in wild type littermates. Moreover, during both awake (dark) and asleep (light) periods, blood pressure was higher in the IC *Nedd4-2* null than the wild type mice (Figure 10A).

We observed some *Nedd4-2* knockdown in cells from IC *Nedd4-2* null kidneys that are not intercalated cells (Figure 2). As such, we cannot exclude the possibility that off-target

Nedd4-2 gene ablation contributes to the increment in blood pressure observed in the IC *Nedd4-2* null mice. Because of this we used an additional approach to examine the effect of IC *Nedd4-2* gene ablation on blood pressure. Pendrin gene ablation eliminates not only pendrin-dependent Cl^-/HCO_3^- exchange, but also downregulates other type B intercalated cell ion transporters that augment the driving force for apical anion exchange, such as the H^+-ATPase (5, 19). We hypothesized that if global *Nedd4-2* gene ablation increases blood pressure in part by upregulating intercalated cell apical anion exchange, then eliminating apical Cl^-/HCO_3^- exchange with pendrin gene ablation should reduce blood pressure more in the global *Nedd4-2* null mice than in mice harboring wild type *Nedd4-2*. To test this hypothesis, we compared blood pressure measured by tailcuff in *Nedd4-2*$^{-/-}$/*Slc26a4*$^{-/-}$; *Nedd4-2*$^{+/+}$/*Slc26a4*$^{-/-}$, *Nedd4-2*$^{-/-}$/*Slc26a4*$^{+/+}$ and wild type mice after 7 days of a 4% NaCl diet (Figure 10B). We observed that blood pressure rose with global *Nedd4-2* gene ablation in mice harboring wild type pendrin (*Slc26a4* $^{+/+}$), as reported previously (47). However, whereas pendrin gene ablation reduced systolic blood pressure in the global *Nedd4-2* null mice, it had no detectable effect on blood pressure in mice harboring wild type *Nedd4-2*. We conclude that the hypertension observed in global *Nedd4-2* null mice occurs, in part, through a mechanism that depends on intercalated cells.

DISCUSSION:

While a human counterpart to the global *Nedd4-2* knockout mice has not been observed, a number of human *NEDD4-2* single nucleotide polymorphisms (SNPs) highly correlate with changes in blood pressure (16). Because *Nedd4-2* is expressed in type B intercalated cells and because intercalated cell function is highly regulated by aldosterone (52), we examined the effect of IC *Nedd4-2* gene ablation on intercalated cell function and how *Nedd4-2*-dependent changes in intercalated cell ion transport impacts blood pressure. We observed that IC *Nedd4-2* gene ablation in mice increases apical Cl^-/HCO_3^- exchange in the CCD and that the increment in blood pressure observed with global *Nedd4-2* gene ablation is in part dependent upon intercalated cells.

Previous studies demonstrated that the ENaC inhibitor, amiloride, eliminates the increment in blood pressure observed with global *Nedd4-2* gene ablation (47). These data might appear at odds with our observation that pendrin gene ablation also eliminates the increment in blood pressure observed in these global *Nedd4-2* KO mice. It is possible that ENaC inhibition mediates the fall in blood pressure seen in both models. *Nedd4-2* gene ablation stimulates both apical Cl^-/HCO_3^- exchange in intercalated cells and ENaC-mediated Na^+ absorption in principal cells (47), which increases renal NaCl absorption. Conversely, amiloride-induced ENaC blockade eliminates ENaC-mediated Na^+ absorption in principal cells, while stimulating HCl secretion by type A intercalated cells (29, 30). Amiloride therefore reduces NaCl absorption and blood pressure. Pendrin gene ablation not only reduces Cl^- absorption by type B and Non-A, non-B intercalated cells (59), but also reduces ENaC-mediated Na^+ absorption (34). Thus, pendrin gene ablation reduces renal NaCl absorption (18, 53) and blood pressure (18), in part through ENaC inhibition.

The global *Nedd4-2* KO mice we studied have a phenotype that appears limited to hypertension (47). However, perinatal lethality is observed in other global *Nedd4-2* null mice (20) that were developed using a floxed *Nedd4-2* mouse in which lox P sites were introduced into a sequence flanking exon 15, thereby inducing a frame shift downstream of exon 15 (20). We chose not to use the latter floxed *Nedd4-2* mice due to the difficulties that arise when studying mice with high perinatal mortality (3, 20). Nevertheless, these data raise the possibility that the global and/or IC *Nedd4-2* null mice we employed might only have a partial loss of *Nedd4-2* function, i.e. hypomorphs, due to alternate splicing (2, 3, 20, 40, 47). If so, the *Nedd4-2*-dependent changes in ion transport we observed would underestimate the true effect of *Nedd4-2* on ion transport.

Nedd4-2 associates with the β or γ subunits of ENaC (1) in a region of the subunit's C terminus having a conserved sequence, known as the PY motif (41, 48). Classical PY motifs, such as those observed in ENaC's β or γ subunits have a C terminal PPPXYXXL sequence, where P is proline, Y is tyrosine, L is leucine and X is any amino acid (6, 37, 41, 48). ClCK-2/barttin is a Cl^- channel that harbors a PPPXYXXL PY motif on the C terminus of the barttin subunit (10). This channel is expressed on the basolateral plasma membrane of both type A and type B intercalated cells of the mouse CCD and is critical to the Cl^- absorption observed in this segment (13, 36). Specifically, the channel's barttin subunit is required for plasma membrane channel expression and therefore channel-mediated Cl^- transport (31), which might occur through a *Nedd4-2* association (10, 31). When the barttin PY motif is mutated and then expressed in heterologous expression systems, increased ClCK-2/barttin-mediated Cl^- channel activity is observed, possibly from the fall in channel ubiquitinylation, endocytosis and degradation that might occur in the absence of a barttin-*Nedd4-2* association (9, 10). The present

study demonstrated, however, that in native intercalated cells, *Nedd4-2* gene ablation does not increase either total or plasma membrane barttin abundance. As such, the interaction of *Nedd4-2* and barttin in vivo and the physiological significance of this association, remains to be determined.

ClC-5 is a Cl^-/H^+ exchanger expressed in the apical regions of intercalated cells (12, 35, 43). Like barttin and ENaC, ClC-5 also harbors a PY motif with a PPLPPY sequence at its C terminus (45). When this PY motif is mutated and then expressed in Xenopus oocytes, ClC-5-mediated current and surface expression increase (45), presumably due to the absence of an interaction with *Nedd4-2* (14). ClC-5 associates with *Nedd4-2* in heterologous expression systems through this PY motif, which reduces ClC-5-mediated current (14). However, following PY motif ablation in the mouse proximal tubule in vivo, no change in ClC-5 subcellular distribution is observed (39). As such, whether this ClC-5-*Nedd4-2* association regulates ClC-5 abundance, subcellular distribution or channel activity in vivo has been unclear. The present study demonstrated that ClC-5 total protein abundance increases with *Nedd4-2* gene ablation in type B, but not in type A, intercalated cells. These data are consistent with previous studies demonstrating greater *Nedd4-2* expression observed in the former than the latter cell type (24). However, the physiological significance of intercalated cell ClC-5 remains to be determined. While mean Cl^- absorption was ~25% lower in CCDs from aldosterone-treated ClC-5 null than wild type littermates, differences did not reach statistical significance (29). As such, whether ClC-5 contributes to the change in Cl^- flux observed with *Nedd4-2* gene ablation and whether it is expressed on the intercalated cell apical plasma membrane, remain to be determined (29).

These ClCK-2/barttin and ClC-5 studies demonstrate that the interaction of *Nedd4-2* with its target proteins can differ in heterologous expression systems and in native tissue. Cultured cells

may lack accessory proteins that are important in protein complexes that occur in native tissue. Moreover, protein overexpression (55) and fluorescent protein tags (54) can lead to nonspecific, off-target effects. As such, occasional associations observed in heterologous expression systems cannot be confirmed in native tissue (39), leaving in question the physiological significance of the initial observations. Given these limitations, we chose to first examine the physiological role of *Nedd4-2* in intercalated cell function by exploring the effect of *Nedd4-2* gene ablation on transporter function in native CCDs and then using these changes in ion transport to predict specific protein targets. We then tested this hypothesis by examining the effect of IC *Nedd4-2* gene ablation on intercalated cell transporter abundance and subcellular distribution in native mouse tissue.

The present study shows that the increase in apical Cl^-/HCO_3^- exchange observed with *Nedd4-2* gene ablation occurs, at least in part, from increased apical plasma membrane pendrin abundance. This increment in apical plasma membrane pendrin abundance occurs primarily through changes in pendrin subcellular distribution rather than through increased pendrin total protein abundance. As such, *Nedd4-2* may represent a step in the aldosterone signaling cascade by which pendrin protein abundance, subcellular distribution, and function are regulated.

While the pendrin does not have a PY motif with a PPXY sequence, it has two PY motifs with LPXY sequences, which might provide recognition motifs for *Nedd4-2* WW domains. One of these, LPKYR, corresponds to amino acids 75-79 of the mouse, rat and human pendrin sequence and amino acids 71-75 in xenopus, providing a potential *Nedd4-2* interaction site (50). However, some proteins, such as the thiazide-sensitive NaCl cotransporter, NCC, associate with *Nedd4-2* independently of a PY motif (2). As such, an intercalated cell transporter such as pendrin might associate with *Nedd4-2* through, or independent of, a C terminal PY motif.

Nedd4-2 gene may target another type B intercalated cell Cl^- transporter not tested in this study. For example, in addition to the type B intercalated cell transporters shown in Figure 1, *Slc26a11* is expressed in intercalated cells and acts as either a Cl^-/HCO_3^- exchanger or a Cl^- channel (62). Whether *Slc26a11* modulates transepithelial ion transport, whether it is expressed on the plasma membrane and whether it is modulated by *Nedd4-2* remain to be determined. Alternatively, *Nedd4-2* might associate with a receptor or a signaling molecule in type B intercalated cells that changes apical anion exchange.

IC *Nedd4-2* gene ablation led to a robust increase in Cl^- absorption without a statistically significant change in transepithelial voltage. However, we cannot exclude the possibility that IC *Nedd4-2* gene ablation produced a small, 1-2 mV, increase in the lumen-negative transepithelial voltage. Since the CCD transports Cl^- through paracellular and transepithelial transport and since *Nedd4-2* enhances paracellular conductance in collecting duct cells by associating with occludin (38), IC *Nedd4-2* gene ablation might alter Cl^- flux through changes in paracellular transport. However, for a change in transepithelial voltage as low as -2 mV to drive significant Cl^- absorption through paracellular transport, there must be a large fall in tubule resistance. This is unlikely because *Nedd4-2* overexpression in cultured CCD cells does not change resistance at steady-state (38). Moreover, if IC *Nedd4-2* gene ablation stimulates occludin-mediated Cl^- absorption, it should also stimulate occludin in the global *Nedd4-2* null mice. Because the lumen-negative voltage is higher in CCDs from the global relative to the IC *Nedd4-2* null mice, we should see a much greater increment in Cl^- absorption in CCDs from the global relative to the IC *Nedd4-2* null mice. Instead, we observed a similar change in Cl^- flux in CCDs from global and IC *Nedd4-2* null mice relative to their wild type controls. We conclude that IC *Nedd4-2* gene ablation changes Cl^- flux in the mouse CCD largely through transcellular transport.

Future experiments will explore whether *Nedd4-2* and pendrin associate and if this association changes apical plasma membrane pendrin ubiquitylation (1, 8, 41). Moreover, since *Nedd4-2* exists as many isoforms due to alternative promoter usage and variable splicing (15), which isoform(s) mediate the *Nedd4-2*-dependent changes in intercalated cell ion transport, also remains to be determined.

In conclusion, IC *Nedd4-2* gene ablation increases electroneutral Cl^-/HCO_3^- exchange in the mouse CCD, partly from pendrin subcellular redistribution, which increases its apical plasma membrane abundance. The increment in blood pressure observed previously in the complete absence of *Nedd4-2* occurs in part through an intercalated cell-dependent mechanism.

AUTHOR CONTRIBUTIONS:

M.N, T.D.P., Y.H.K., R.L.S., K.I.L.-C., R.C., A.Y.P., V.P., J.W.V. performed experiments. B.Y., O.S., J.D.K., X.W. and S.M.W. contributed to the conception and design of the experiments and its analysis. S.M.W. drafted and revised the manuscript. All authors provided feedback on the manuscript and approved its final version. All authors agree to be accountable for the work.

ACKNOWLEDGEMENTS:

This study was supported by DK 104125 and AHA 15GRNT25710001 (to S.M.W). R Chambrey is funded by grant ANR BLANC 2012-R13011KK from l'Agence Nationale de la Recherche (ANR); K.I.L.-C. received a fellowship from the Comisión Nacional de Investigación Científica y Tecnológica (CONICYT). We thank Drs. Raoul Nelson, R. Lance Miller, John Stokes and I. David Weiner for providing the B1-H^+-ATPase Cre and the floxed *Nedd4-2* mice. We thank Dr. Greg L. Shipley (Shipley Consulting LLC, Austin, TX) for his assistance with primer design. We thank Drs. Thomas Jentsch, Christian Hubner and Fiona Karet for providing the barttin, AE4 and α4 H^+-ATPase antibodies.

REFERENCES

1. **Abriel H, Loffing J, Rebhun JF, Pratt JH, Schild L, Horisberger JD, Rotin D, and Staub O.** Defective regulation of the epithelial Na+ channel by Nedd4 in Liddle's syndrome. *J Clin Invest* 103: 667-673, 1999.

2. **Arroyo JP, Lagnaz D, Ronzaud C, Vazquez N, Ko BS, Moddes L, Ruffieux-Daidie D, Hausel P, Koesters R, Yang B, Stokes JB, Hoover RS, Gamba G, and Staub O.** Nedd4-2 modulates renal Na^+-Cl^- cotransporter via the aldosterone-Sgk1-Nedd4-2 pathway. *JAmSocNephrol* 22: 1707-1719, 2011.

3. **Boase NA, Rychkov GY, Townley SL, Dinudom A, Candi E, Voss AK, Tsoutsman T, Semsarian C, Melino G, Koentgen F, Cook DI, and Kumar S.** Respiratory distress and perinatal lethality in Nedd4-2-deficient mice. *Nat Commun* 2: 287, 2011.

4. **Brown D, Hirsch S, and Gluck S.** Localization of a proton-pumping ATPase in rat kidney. *JClinInvest* 82: 2114-2126, 1988.

5. **Chambrey R, Kurth I, Peti-Peterdi J, Houillier P, Purkerson JM, Leviel F, Hentschke M, Zdebik AA, Schwartz GJ, Hubner CA, and Eladari D.** Renal intercalated cells are rather energized by a proton than a sodium pump. *Proc Natl Acad Sci U S A* 110: 7928-7933, 2013.

6. **Dahlmann A, Pradervand S, Hummler E, Rossier BC, Frindt G, and Palmer LG.** Mineralocorticoid regulation of epithelial Na+ channels is maintained in a mouse model of Liddle's syndrome. *AmJPhysiol* 285: F310-F318, 2003.

7. **Debonneville C, Flores SY, Kamynina E, Plant PJ, Tauxe C, Thomas MA, Munster C, Chraibi A, Pratt JH, Horisberger J-D, Pearce D, Loffing J, and Staub O.** Phosphorylation of Nedd4-2 by Sgk1 regulates epithelial Na+ channel cell surface expression. *Embo J* 20: 7052-7059, 2001.

8. **Eaton DC, Malik B, Bao H-F, Yu L, and Jain L.** Regulation of epithelial sodium channel trafficking by ubiquitination. *ProcAmThoracSoc* 7: 54-64, 2010.

9. **Embark HM, Bohmer C, Palmada M, Rajamanickam J, Wyatt AW, Wallisch S, Capasso G, Waldegger P, Seyberth HW, Waldegger S, and Lang F.** Regulation of CLC-Ka/barttin by the ubiquitin ligase Nedd4-2 and the serum and glucocorticoid-dependent kinases. *Kidney Int* 66: 1918-1925, 2004.

10. **Estevez R, Boettger T, Stein V, Birkenhager R, Otto E, Hildebrandt F, and Jentsch TJ.** Barttin is a Cl^- channel β subunit-crucial for renal Cl- reabsorption and inner ear K^+ secretion. *Nature* 414: 558-561, 2001.

11. **Flores SY, Loffing-Cueni D, Kamynina E, Daidie D, Gerbex C, Chabanel S, Dudler J, Loffing J, and Staub O.** Aldosterone-induced serum and glucocorticoid-induced kinase 1 expression is accompanied by Nedd4-2 phosphorylation and increased Na+ transport in cortical collecting duct cells. *JAmSocNephrol* 16: 2279-2287, 2005.

12. **Gunther W, Luchow A, Cluzeaud F, Vandewalle A, and Jentsch TJ.** ClC-5, the chloride channel mutated in Dent's disease, colocalizes with the proton pump in endocytotically active kidney cells. *ProcNatlAcadSciUSA* 95: 8075-8080, 1998.

13. **Hennings JC, Andrini O, Picard N, Paulais M, Huebner AK, Cayuqueo IK, Bignon Y, Keck M, Corniere N, Bohm D, Jentsch TJ, Chambrey R, Teulon J, Hubner CA, and Eladari D.** The ClC-K2 Chloride Channel Is Critical for Salt Handling in the Distal Nephron. *J Am Soc Nephrol*, 2016.

14. **Hryciw DH, Ekberg J, Lee A, Lensink IL, Kumar S, Guggino WB, Cook DI, Pollock CA, and Poronnik P.** Nedd4-2 functionally interacts with ClC-5: involvement in constitutive albumin endocytosis in proximal tubule cells. *J Biol Chem* 279: 54996-55007, 2004.

15. **Itani OA, Stokes JB, and Thomas CP.** Nedd4-2 isoforms differentially associate with ENaC and regulate its activity. *AmJPhysiol* 289: F334-F346, 2005.

16. **Jin H-S, Hong KW, Lim J-E, Hwang S-Y, Lee S-H, Shin C, Park HK, and Oh B.** Genetic variations in the sodium balance-regulating genes ENaC, NEDD4L, NDFIP2 and USP2 influence blood pressure and hypertension. *Kidney Blood PressRes* 33: 15-23, 2010.

17. **Kim G-H, Masilamani S, Turner R, Mitchell C, Wade JB, and Knepper MA.** The thiazide-sensitive Na-Cl cotransporter is an aldosterone-induced protein. *ProcNatlAcadSciUSA* 95: 14552-14557, 1998.

18. **Kim Y-H, Pech V, Spencer KB, Beierwaltes WH, Everett LA, Green ED, Shin WK, Verlander JW, Sutliff RL, and Wall SM.** Reduced ENaC expression contributes to the lower blood pressure observed in pendrin null mice. *AmJPhysiol* 293: F1314-F1324, 2007.

19. **Kim Y-H, Verlander JW, Matthews SW, Kurtz I, Shin WK, Weiner ID, Everett LA, Green ED, Nielsen S, and Wall SM.** Intercalated cell H+/OH- transporter expression is reduced in *Slc26a4* null mice. *AmJPhysiol* 289: F1262-F1272, 2005.

20. **Kimura T, Kawabe H, Jiang C, Zhang W, Xiang YY, Lu C, Salter MW, Brose N, Lu WY, and Rotin D.** Deletion of the ubiquitin ligase Nedd4L in lung epithelia causes cystic fibrosis-like disease. *Proc Natl Acad Sci U S A* 108: 3216-3221, 2011.

21. **Kurtz TW, Hamoudi AA-B, and Morris RC.** "Salt-sensitive" essential hypertension in men. *NEnglJMed* 317: 1043-1048, 1987.

22. **Kurtz TW and Morris RC.** Dietary chloride as a determinant of "sodium-dependent" hypertension. *Science* 222: 1139-1141, 1983.

23. **Leviel F, Hubner CA, Houillier P, Morla L, El Moghrabi S, Brideau G, Hatim H, Parker MD, Kurth I, Kougioumtzes A, Sinning A, Pech V, Riemondy KA, Miller RL, Hummler E, Shull GE, Aronson PS, Doucet A, Wall SM, Chambrey R, and Eladari D.** The Na^+-dependent chloride-bicarbonate exchanger SLC4A8 mediates an electroneutral Na+ reabsorption process in the renal cortical collecting ducts of mice. *JClinInvest* 120: 1627-1635, 2010.

24. **Loffing-Cueni D, Flores SY, Sauter D, Daidie D, Siegrist N, Meneton P, Staub O, and Loffing J.** Dietary sodium intake regulates the ubiquitin-proteinligase Nedd4-2 in the renal collecting system. *JAmSocNephrol* 17: 1264-1274, 2006.

25. **Masilamani S, Kim G-H, Mitchell C, Wade JB, and Knepper MA.** Aldosterone-mediated regulation of ENaC α,β and γ subunit proteins in rat kidney. *JClinInvest* 104: R19-R23, 1999.

26. **Miller RL, Lucero OM, Riemondy KA, Baumgartner BK, Brown D, Breton S, and Nelson RD.** The V-ATPase B1-subunit promoter drives expression of Cre recombinase in intercalated cells of the kidney. *Kidney Int* 75: 435-439, 2009.

27. **Miller RL, Zhang P, Smith M, Beaulieu V, Paunescu TG, Brown D, Breton S, and Nelson RD.** V-ATPase B1-subunit promoter drives expression of EGFP in intercalated cells of kidney, clear cells of epididymis and airway cells of lung in transgenic mice. *AmJPhysiol* 288: C1134-C1144, 2005.

28. **Muzumdar MD, Tasic B, Miyamichi K, Li L, and Luo L.** A global double-fluorescent Cre reporter mouse. *Genesis* 45: 593-605, 2007.

29. **Nanami M, Lazo-Fernandez Y, Pech V, Verlander JW, Agazatian D, Weinstein AM, Bao HF, Eaton DC, and Wall SM.** ENaC inhibition stimulates HCl secretion in the mouse cortical collecting duct I: stilbene-sensitive Cl- secretion. *Am J Physiol Renal Physiol* 309: F251-F258, 2015.

30. **Nanami M, Pech V, Lazo-Fernandez Y, Weinstein AM, and Wall SM.** ENaC inhibition stimulates HCl secretion in the mouse cortical collecting duct II: Bafilomycin-sensitive H+ secretion. *Am J Physiol Renal Physiol* 309: F259-268, 2015.

31. **Nomura N, Tajima M, Sugawara N, Morimoto T, Kondo Y, Ohno M, Uchida K, Mutig K, Bachmann S, Soleimani M, Ohta E, Ohta A, Sohara E, Okado T, Rai T, Jentsch TJ, Sasaki S, and Uchida S.** Generation and analyses of R8L barttin knockin mouse. *AmJPhysiol* 301: F297-F307, 2011.

32. **Pech V, Kim Y-H, Weinstein AM, Everett LA, Pham TD, and Wall SM.** Angiotensin II increases chloride absorption in the cortical collecting duct in mice through a pendrin-dependent mechanism. *AmJPhysiol* 292: F914-F920, 2007.

33. **Pech V, Thumova M, Kim Y-H, Agazatian D, Hummler E, Rossier BC, Weinstein AM, Nanami M, and Wall SM.** ENaC inhibition stimulates Cl^- secretion in the mouse cortical collecting duct through an NKCC1-dependent mechanism. *AmJPhysiol* 303: F45-F55, 2012.

34. **Pech V, Wall SM, Nanami M, Bao HF, Kim YH, Lazo-Fernandez Y, Yue Q, Pham TD, Eaton DC, and Verlander JW.** Pendrin gene ablation alters ENaC subcellular distribution and open probability. *Am J Physiol Renal Physiol* 309: F154-163, 2015.

35. **Picollo A and Pusch M.** Chloride/proton antiporter activity of mammalian CLC proteins ClC-4 and ClC-5. *Nature* 436: 420-423, 2005.

36. **Pinelli L, Nissant A, Edwards A, Lourdel S, Teulon J, and Paulais M.** Dual regulation of the native ClC-K2 chloride channel in the distal nephron by voltage and pH. *J Gen Physiol* 148: 213-226, 2016.

37. **Pradervand S, Wang Q, Burnier M, Beermann F, Horisberger JD, Hummler E, and Rossier BC.** A mouse model for Liddle's Syndrome. *JAmSocNephrol* 10: 2527-2533, 1999.

38. **Raikwar NS, Vandewalle A, and Thomas CP.** Nedd4-2 interacts with occludin to inhibit tight junction formation and enhance paracellular conductance in collecting duct epithelia. *Am J Physiol Renal Physiol* 299: F436-444, 2010.

39. **Rickheit G, Wartosch L, Schaffer S, Stobrawa SM, Novarino G, Weinert S, and Jentsch TJ.** Role of ClC-5 in renal endocytosis is unique among ClC exchangers and does not require PY-motif-dependent ubiquitylation. *J Biol Chem* 285: 17595-17603, 2010.

40. **Ronzaud C, Loffing-Cueni D, Hausel P, Debonneville A, Malsure SM, Fowler-Jaeger N, Bobadilla NA, Perrier R, Maillard M, Yang B, Stokes JB, Koesters R, Kumar S, Hummler E, Loffing J, and Staub O.** Renal tubular NEDD4-2 deficiency causes NCC-mediated salt-dependent hypertension. *JClinInvest*, 2013.

41. **Rotin D and Staub O.** Role of the ubiquitin system in regulating ion transport. *Pflugers Arch* 461: 1-21, 2011.

42. **Royaux IE, Wall SM, Karniski LP, Everett LA, Suzuki K, Knepper MA, and Green ED.** Pendrin, encoded by the pendred syndrome gene, resides in the apical region of renal intercalated cells and mediates bicarbonate secretion. *ProcNatlAcadSciUSA* 98: 4221-4226, 2001.

43. **Scheel O, Zdebik AA, Lourdel S, and Jentsch TJ.** Voltage-dependent electrogenic chloride/proton exchange by endosomal CLC proteins. *Nature* 436: 424-427, 2005.

44. **Schlatter E, Greger R, and Schafer JA.** Principal cells of cortical collecting ducts of the rat are not a route of transepithelial Cl^- transport. *Pflugers Arch* 417: 317-323, 1990.

45. **Schwake M, Friedrich T, and Jentsch TJ.** An internalization signal in ClC-5, an endosomal Cl-channel mutated in dent's disease. *J Biol Chem* 276: 12049-12054, 2001.

46. **Shcheynikov N, Yang D, Wang Y, Zeng W, Karniski LP, So I, Wall SM, and Muallem S.** Slc26a4 functions as an electroneutral Cl-/I-/HCO3- exchanger: role of Slc26a4 and Slc26a6 in I- and HCO3- secretion and in regulation of CFTR in the parotid duct. *JPhysiol* 586: 3814-3824, 2008.

47. **Shi PP, Cao XR, Sweezer EM, Kinney TS, Williams NR, Husted RF, Nair R, Weiss RM, Williamson RA, Sigmund CD, Snyder PM, Staub O, Stokes JB, and Yang B.** Salt-sensitive hypertension and cardiac hypertrophy in mice deficient in the ubiquitin ligase Nedd4-2. *AmJPhysiol* 295: F462-F470, 2008.

48. **Snyder PM.** Down-regulating destruction; phosphorylation regulates the E3 ubiquitin ligase Nedd4-2. *SciSignal* 2: 1-3, 2009.

49. **Star RA, Burg MB, and Knepper MA.** Bicarbonate secretion and chloride absorption by rabbit cortical collecting ducts: role of chloride/bicarbonate exchange. *JClinInvest* 76: 1123-1130, 1985.

50. **Staub O and Rotin D.** Role of ubiquitinylation in cellular membrane transport. *PhysiolRev* 86: 669-707, 2006.

51. **Terada Y and Knepper MA.** Thiazide-sensitive NaCl absorption in rat cortical collecting duct. *AmJPhysiol* 259: F519-F528, 1990.

52. **Verlander JW, Hassell KA, Royaux IE, Glapion DM, Wang ME, Everett LA, Green ED, and Wall SM.** Deoxycorticosterone upregulates PDS (Slc26a4) in mouse kidney: role of pendrin in mineralocorticoid-induced hypertension. *Hypertension* 42: 356-362, 2003.

53. **Verlander JW, Kim YH, Shin W, Pham TD, Hassell KA, Beierwaltes WH, Green ED, Everett L, Matthews SW, and Wall SM.** Dietary Cl(-) restriction upregulates pendrin expression within the apical plasma membrane of type B intercalated cells. *Am J Physiol Renal Physiol* 291: F833-839, 2006.

54. **Viallet PM and Vo-Dinh T.** Monitoring intracellular proteins using fluorescence techniques: from protein synthesis and localization to activity. *CurrProtein PeptSci* 4: 375-388, 2003.

55. **Wall JG and Pluckthun A.** Effects of overexpressing folding modulators on the in vivo folding of heterologous proteins in Escherichia coli. *CurrOpinBiotechnol* 6: 507-516, 1995.

56. **Wall SM and Fischer MP.** Contribution of the Na^+-K^+-$2Cl^-$ cotransporter (NKCC1) to transepithelial transport of H^+, NH_4^+, K^+ and Na^+ in rat outer medullary collecting duct. *JAmSocNephrol* 13: 827-835, 2002.

57. **Wall SM, Fischer MP, Mehta P, Hassell KA, and Park SJ.** Contribution of the Na^+-K^+-$2Cl^-$ cotransporter (NKCC1) to Cl^- secretion in rat outer medullary collecting duct. *AmJPhysiol* 280: F913-F921, 2001.

58. **Wall SM, Hassell KA, Royaux IE, Green ED, Chang JY, Shipley GL, and Verlander JW.** Localization of pendrin in mouse kidney. *AmJPhysiol* 284: F229-F241, 2003.

59. **Wall SM, Kim YH, Stanley L, Glapion DM, Everett LA, Green ED, and Verlander JW.** NaCl restriction upregulates renal Slc26a4 through subcellular redistribution: role in Cl-conservation. *Hypertension* 44: 982-987, 2004.

60. **Wall SM and Weinstein AM.** Cortical distal nephron Cl(-) transport in volume homeostasis and blood pressure regulation. *Am J Physiol Renal Physiol* 305: F427-438, 2013.

61. **Wen H, Lin R, Jiao Y, Wang F, Wang S, Lu D, Qian J, Jin L, and Wang X.** Two polymorphisms in NEDD4L gene and essential hypertension in Chinese Hans-A population-based case-control study. *ClinExpHypertens* 30: 87-94, 2008.

62. **Xu J, Barone S, Li H, Holiday S, Zahedi K, and Soleimani M.** Slc26a11, a chloride transporter, localizes with the vacuolar H^+-ATPase of A-intercalated cells of the kidney. *Kidney Int* 80: 926-937, 2011.

Table 1: *Nedd4-2* immunolabel in the mouse CCD cell types taken from Cre (+), intercalated cell (IC) *Nedd4-2* null and Cre (-), wild type littermates following 7 days of a NaCl-rich diet (1.4 meq/day NaCl).

	Principal Cells		Intercalated Cells	
	% *Nedd4-2* positive	% *Nedd4-2* negative	% *Nedd4-2* positive	% *Nedd4-2* negative
Cre (+), IC *Nedd4-2* null, n=4	88.4 ± 1.6	11.6 ± 1.6	28.5 ± 2.5	71.5 ± 2.6
Cre (-), Wild type, n=3	87.6 ± 4.6	12.3 ± 4.6	74.1 ± 7.6	28.0 ± 6.1

Each "n" represents counts from separate mice.

Table 2: Effect of IC *Nedd4-2* gene ablation on serum electrolytes, arterial blood gases and serum aldosterone.

	Cre (-), floxed *Nedd4-2*, wild type	Cre (+), IC *Nedd4-2* null	P
Na^+, meq/l	144 ± 1 (n=4)	144 ± 1 (n=4)	NS
K^+, meq/l	3.3 ± 0.2 (n=4)	3.0 ± 0.2 (n=4)	NS
Cl^-, meq/l	115 ± 1 (n=4)	115 ± 1 (n=4)	NS
HCO_3^-, meq/l	20 ± 1 (n=4)	21 ± 1 (n=4)	NS
Aldosterone, nM	2.3 ± 0.5 (n=12)	1.6 ± 0.4 (n=14)	NS
Arterial pH	7.50 ± 0.02 (n=4)	7.47 ± 0.01 (n=4)	NS
pCO_2	25.2 ± 1	27.7 ± 1	NS
$cHCO_3^-$	19.4 ± 0.5	19.9 ± 0.8	NS

Each "n" represents values from separate mice. Mice consumed the NaCl-rich diet (1.4 meq/d NaCl) for 7 days before sacrifice.

Table 3: Effect of IC *Nedd4-2* gene ablation on apical plasma membrane and cytoplasm pendrin abundance in mouse CCD and CNT.

	Type B		Non-A, Non-B	
	Wild type	IC *Nedd4-2* KO	Wild type	IC *Nedd4-2* KO
No. of mice studied	8	9	4	5
Apical plasma membrane gold label, gold particles/cell	7.84 ± 1.59	13.1 ± 3.0	26.5 ± 4.8	47.6 ± 4.1*
Cytoplasmic gold, gold particles in cytoplasm/cell	71.1 ± 1.28	53.6 ± 0.76	76.0 ± 19.8	76.6 ± 8.9
Total gold	79.0 ± 13.6	66.7 ± 8.8	102 ± 22	124 ± 11
Ratio of apical plasma membrane to cytoplasm pendrin label, x 10^{-1}	1.24 ± 0.29	2.63 ± 0.51*	4.6 ± 2.0	6.4 ± 0.7
Apical plasma membrane boundary length, mm x 10^{-2}	0.72 ± 0.07	1.02 ± 0.11*	3.04 ± 0.49	4.49 ± 0.36*
Apical plasma membrane label density, gold particles/mm apical plasma membrane boundary length x 10^{3}	1.27 ± 0.39	1.19 ± 0.18	1.02 ± 0.09	1.17 ± 0.15
Cell area, mm^2 x 10^{-5}	4.39 ± 0.20	4.65 ± 0.33	4.86 ± 0.43	4.85 ± 0.55
Cytoplasmic label density, gold particles x $10^{6}/mm^{2}$ cytoplasmic area	1.69 ± 0.36	1.19 ± 1.71	1.59 ± 0.32	1.66 ± 0.19

Values were determined using immunogold cytochemistry with morphometric analysis and represent the means ± SE. Values were compared with an unpaired, two-tailed Student's t-test. *$P < 0.05$. Mice consumed the NaCl-rich diet (1.4 meq/d NaCl) for 7 days before sacrifice.

FIGURE LEGENDS

Figure 1: Ion transporters in mouse cortical collecting duct. Mouse CCD is made up of principal cells, which mediate electrogenic Na^+ absorption through the benzamil-sensitive Epithelial Na^+ channel on the apical plasma membrane. Na^+ exits principal cells across the basolateral plasma membrane through the Na,K-ATPase. ENaC-mediated Na^+ absorption creates a lumen-negative voltage, which provides the driving force for K^+ secretion. Type B intercalated cells mediate electroneutral NaCl absorption and HCO_3^- secretion through an apical plasma membrane Na^+-independent electroneutral Cl^-/HCO_3^- exchanger, that acts in tandem with a Na^+-dependent Cl^-/HCO_3^- exchanger. NaCl exits the cell through a basolateral plasma membrane Cl^- channel and a $NaHCO_3$ cotransporter. Net H^+ equivalents exit across the basolateral plasma membrane through the H^+-ATPase. The Type A intercalated cell mediates uptake of H^+ equivalents and Cl^- across the basolateral plasma membrane through a Na^+-K^+-$2Cl^-$ cotransporter, Cl^-/HCO_3^- exchange (AE1) and possibly a Cl^- channel. This cell type secretes HCl through an apical H^+-ATPase and an apical Cl^- channel or Cl^-/HCO_3^- exchanger.

Figure 2: Cre recombinase is expressed primarily within intercalated cells of the IC *Nedd4-2* KO mice. IC *Nedd4-2* null mice were bred to Cre reporter mice (Td Tomato). The resulting B1-ATPase Cre (+), dTomato (+/-) offspring were studied after 7 days of the gelled diet (1.4 meq/day NaCl). dTomato immunofluorescence (red) reflects Cre recombinase expression in that cell. Panel A shows intercalated cells identified by combined pendrin and AE1 labeling (green) in a representative CCD and CNT. Basolateral green immunofluorescence (solid arrowheads) indicates basolateral AE1 expression, a marker of type A ICs, while apical green fluorescence

labeling (solid arrows) indicates pendrin expression, a marker of type B and Non-A, non-B ICs. In the CCD (A, upper panel), green and red fluorescence are observed in the same cells, indicating that Cre recombinase expression is restricted to intercalated cells. In the CNT (A, lower panel), rare AE1/pendrin negative cells (CNT cells) express strong dTomato/Cre recombinase (open arrowheads), although the majority of the CNT cells either have no dTomato fluorescence (asterisks) or have faint dTomato fluorescence (open arrows).

We also observed occasional dTomato fluorescence outside the collecting duct and connecting tubule. While not all cell types could be identified in these images, dTomato was sometimes observed in glomeruli (Panel B), blood vessels (Panel B) and in some cells within the interstitium (Panel C).

Figure 3: *Nedd4-2* labeling is reduced in intercalated cells taken from CCDs of IC *Nedd4-2* KO mice. This slide shows cortical sections from a *Nedd4-2* KO and a wild type littermate labeled for AQP2 (blue, a principal cell marker) and *Nedd4-2* (brown). Asterisks mark AQP2-positive (principal) cells, whereas arrows show AQP2-negative (intercalated) cells. In cortical sections from wild type mice, *Nedd4-2* label was observed in both intercalated and in principal cells. However, in the IC *Nedd4-2* null mice, while *Nedd4-2* label was seen in principal cells, *Nedd4-2* label was observed in only rare intercalated cells (AQP2-negative cells).

Figure 4: Global, but not intercalated cell-specific, *Nedd4-2* gene ablation increases benzamil-sensitive V_T. The benzamil-sensitive component of V_T was calculated and used as an indicator of ENaC-mediated Na^+ absorption. Benzamil-sensitive V_T was low and not significantly different in CCDs from IC *Nedd4-2* KO (n=3) and wild type littermates (Cre (-),

floxed *Nedd4-2* mice, n=3, Left Panel). In contrast, benzamil-sensitive V_T was much higher in CCDs from global *Nedd4-2* null mice (n=3) relative to wild type, C57Bl/6 controls (n=4; Right Panel).

Figure 5: IC *Nedd4-2* gene ablation increases electroneutral Cl^-/HCO_3^- exchange. Cl^- (J_{Cl}) and tCO2 (J_{tCO2}) flux as well as transepithelial voltage, V_T, were measured in IC *Nedd4-2* KO and the Cre (-), floxed *Nedd4-2* littermates (wild type littermates, Panel A). As shown, CCDs from wild type littermates secrete Cl^- (n=4) and absorb tCO_2(n=5). In contrast, CCDs from IC *Nedd4-2* null mice absorb Cl^- (n=4) and secrete tCO_2 (n=4). V_T, however, was unchanged with IC *Nedd4-2* gene ablation (n=8 wild type and n=8 IC *Nedd4-2* null mice). Panel B shows that *Nedd4-2* gene ablation in both principal and intercalated cells (n=3) produced a similar increase in Cl^- absorption, J_{Cl}, relative to wild type controls (C57Bl/6, n=4). Transepithelial voltage, V_T, was -2.2 ± 0.84 (n=4) in C57 Bl/6, wild type mice and -10.3 ± 4.0 (n=3) mV in global *Nedd4-2* null mice.

Figure 6: Thiazide-sensitive J_{Cl} and thiazide-sensitive Na^+-dependent Cl^-/HCO_3^- exchanger (NDCBE, *Slc4a8*) abundance do not increase markedly with IC *Nedd4-2* gene ablation. Cl^- absorption, J_{Cl} was measured in CCDs from IC *Nedd4-2* null (n=13) and wild type littermates (n=8) with 100 μM hydrochlorothiazide (HCTZ) or vehicle (Veh) added to the perfusate (Panel A). Solid lines indicate experiments where vehicle was present in the first period and HCTZ added in the second. The dashed lines show the reverse order, i.e. HCTZ present in period one and then removed in period two. Panel B compares thiazide-sensitive J_{Cl} in CCDs from both groups.

Panel C shows NDCBE protein abundance in plasma membrane-enriched preparations from the renal cortex of IC *Nedd4-2* null and wild type littermates**.** Each lane was loaded with a protein sample from a different mouse. 15 μg proteins were loaded per gel lane with equal loading was confirmed by parallel Coomassie-stained gels (Panel D). The anti NDCBE antibody recognized a band at 130 kDa. Densitometric values were normalized to the mean for the Cre (-), wild type littermates.

Figure 7: IC *Nedd4-2* gene ablation does not increase the benzamil-sensitive component of J_{Cl}. Cl^- absorption, J_{Cl}, was measured in CCDs from IC *Nedd4-2* null (n=15) and wild type littermates (n=11) with 3 μM benzamil (Benz) or vehicle (Veh) in the perfusate (Panel A). The solid lines indicate experiments where vehicle was present in the first period and benzamil added in the second. The dashed lines show the reverse order, i.e. benzamil present in period one and then removed in period two. Panel B compares benzamil-sensitive J_{Cl} in CCDs from mice in each group.

Figure 8: *Nedd4-2* gene ablation increases total ClC-5 label in type B intercalated cells and increase its relative label in the region of the apical plasma membrane. Panel A shows ClC-5 and AE1 labeling in a renal cortical sections from a wild type and a global *Nedd4-2* null littermate. In other experiments not shown, cortical sections were labeled for ClC-5 and pendrin. ClC-5 abundance was quantified in both type A (AE1 positive, pendrin negative, open arrows) and B intercalated cells (AE1 negative, pendrin positive, solid arrows). Panels B & C show that *Nedd4-2* gene ablation did not increase either total ClC-5 abundance per cell or ClC-5 label in the apical membrane region of type A intercalated cells. However, in type B intercalated cells

(Panels D & E), global *Nedd4-2* gene ablation increased both ClC-5 abundance per cell as well as the relative abundance of ClC-5 in the apical membrane region.

Figure 9: Pendrin protein abundance is not significantly changed with IC *Nedd4-2* gene ablation. Cortical sections from a representative IC *Nedd4-2* KO and wild type littermate were labeled for pendrin. Panels A & D show pendrin labeling at low magnification. The insets show typical CNTs (Panels B & E) and typical CCDs (Panels C and F) at higher magnification.

Panel G shows a representative immunoblot of kidney lysates from IC *Nedd4-2* KO and wild type littermates probed for pendrin and its respective Coomassie blue gel, which confirms protein loading (Panel H). Panel I demonstrates that pendrin band density is similar in kidney lysates from IC *Nedd4-2* null and wild type littermates. Panel J shows that kidney pendrin (*Slc26a4*) mRNA when normalized to 18S mRNA is the same or reduced with IC *Nedd4-2* gene ablation.

Figure 10: Intercalated cells contribute to the increment in blood pressure observed with *Nedd4-2* gene ablation. Panel A shows mean arterial pressure (MAP) measured by radiotelemetry after 7 days of a 4% NaCl diet. As shown, MAP was higher in the IC *Nedd4-2* null (n=4) relative to wild type littermates (n=5) during both awake (dark periods, 6 p to 6 am) and during asleep (light, 6 am to 6 pm) periods. Panel B shows systolic blood pressure measured by tailcuff in wild type ($Slc26a4^{+/+}/Nedd4\text{-}2^{+/+}$), pendrin null ($Slc26a4^{-/-}/Nedd4\text{-}2^{+/+}$), *Nedd4*-2 null ($Slc26a4^{+/+}/Nedd4\text{-}2^{-/-}$) and in mice that were both pendrin and *Nedd4-2* null ($Slc26a4^{-/-}$

/*Nedd4-2*$^{-/-}$) mice after consuming a 4% NaCl diet at libitum for 6 days. Measurements were made in 5 mice from each group. *P< 0.05.

Figure 1

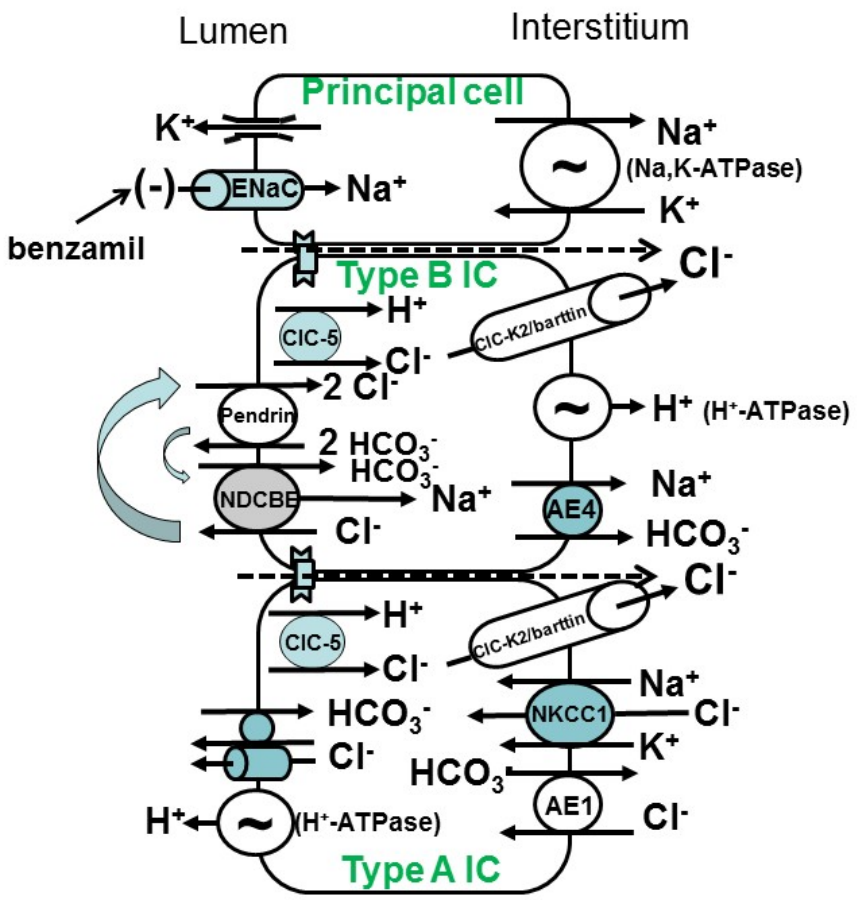
Lumen
Interstitium
Principal cell
K+
Na+
(Na,K-ATPase)
(-)
ENaC
Na+
K+
benzamil
Cl-
Type B IC
H+
ClC-5
ClC-K2/barttin
Cl-
2 Cl-
Pendrin
H+ (H+-ATPase)
2 HCO3-
HCO3-
NDCBE
Na+
Na+
AE4
Cl-
HCO3-
Cl-
H+
ClC-5
ClC-K2/barttin
Cl-
Na+
HCO3-
NKCC1
Cl-
Cl-
K+
HCO3-
AE1
H+
(H+-ATPase)
Cl-
Type A IC

Figure 2

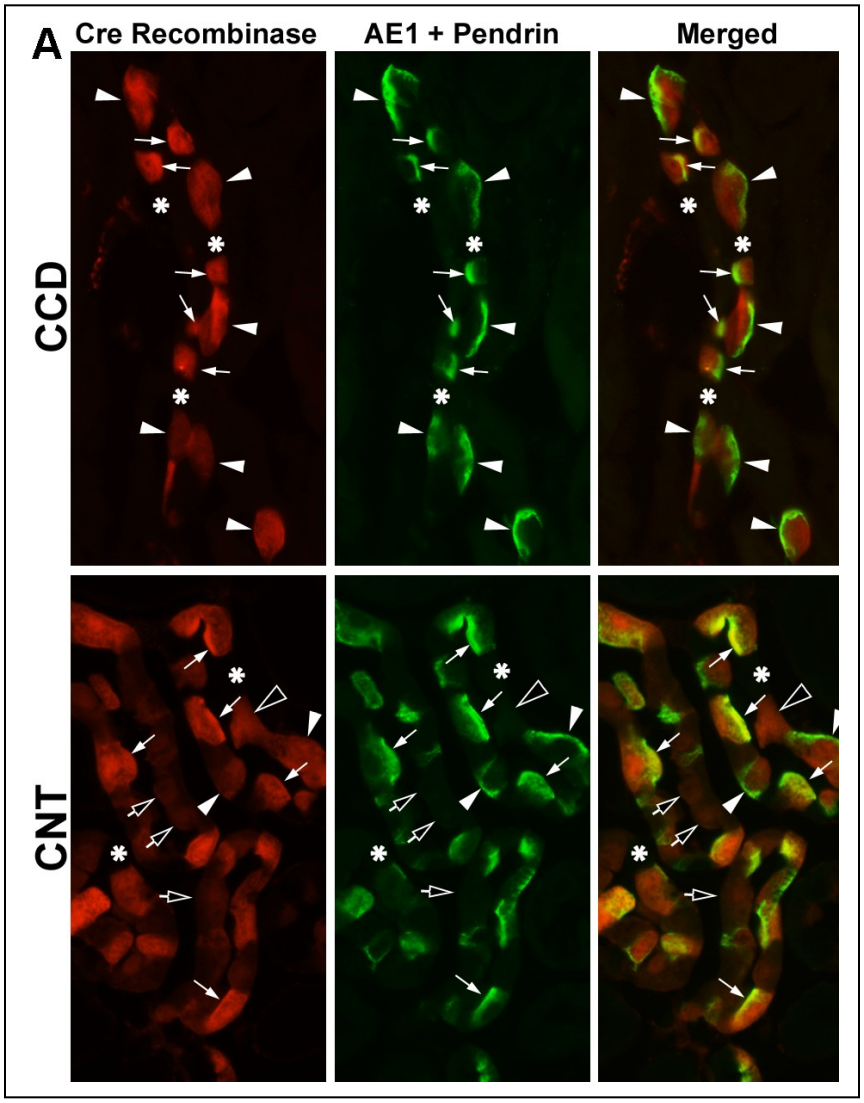
A
Cre Recombinase
AE1 + Pendrin
Merged
CCD
CNT

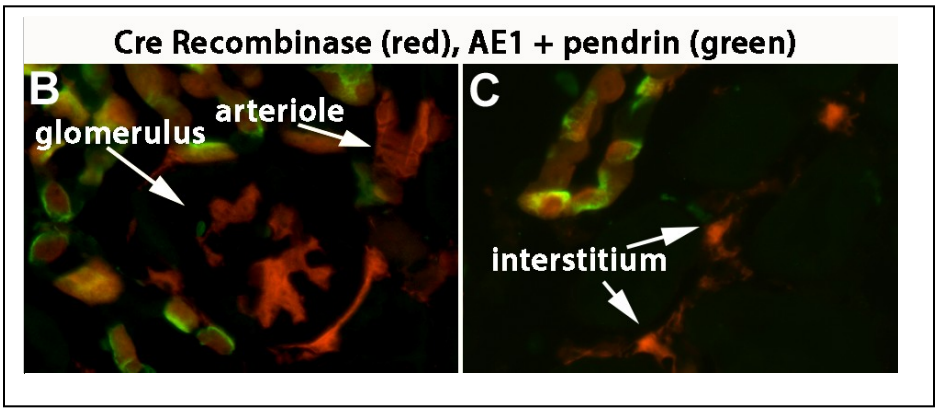
Cre Recombinase (red), AE1 + pendrin (green)
B
glomerulus
arteriole
C
interstitium

Figure 3

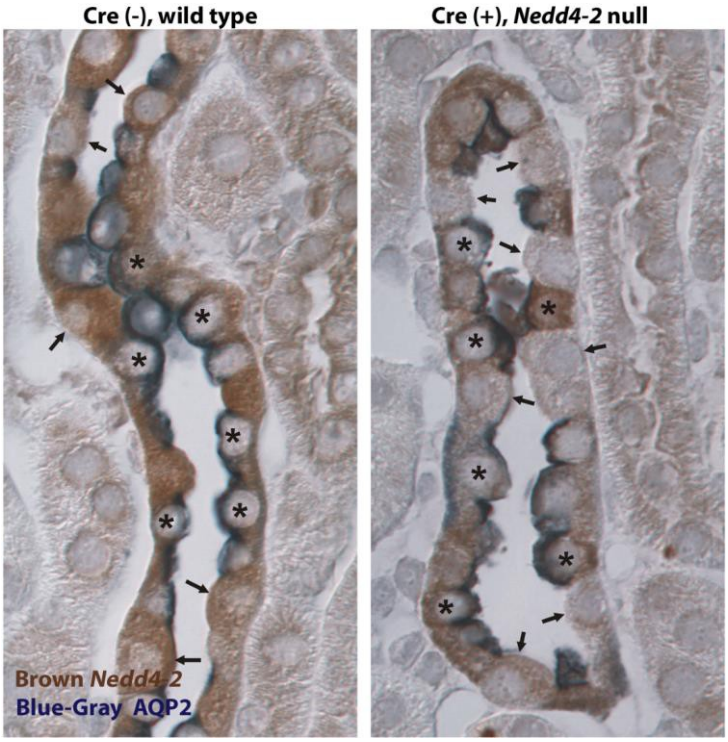

Figure 4

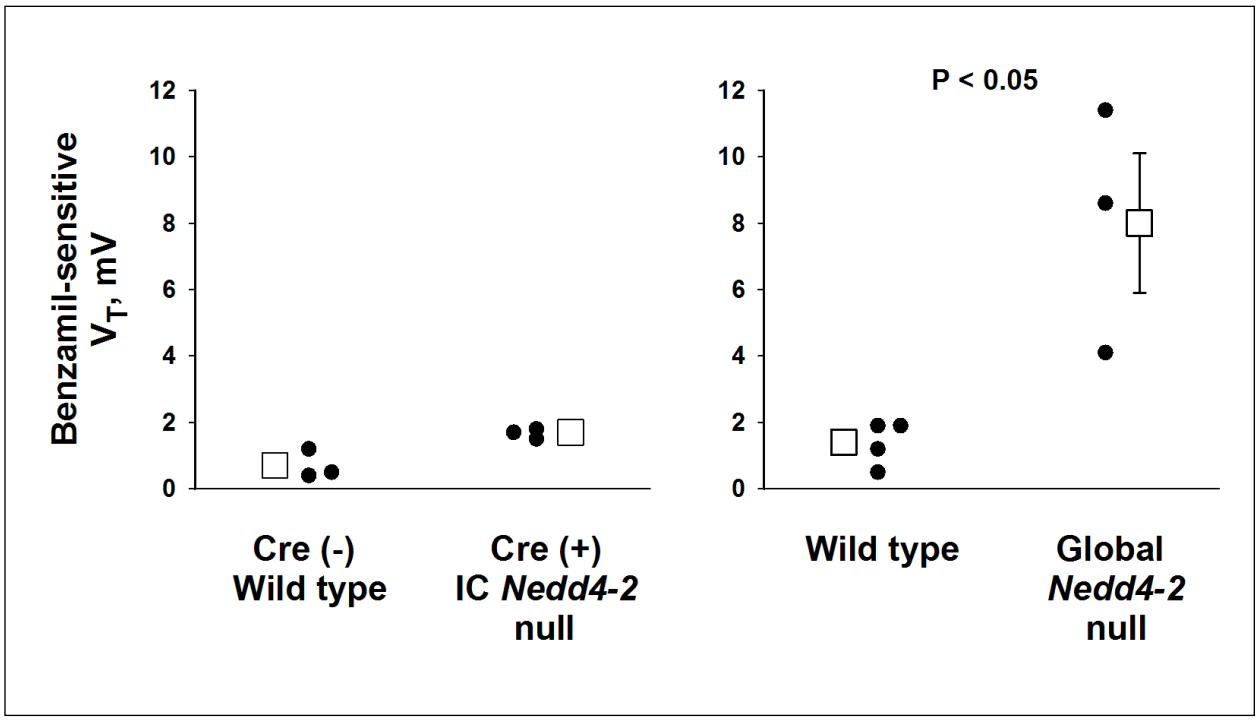
Benzamil-sensitive
V_T, mV
12
10
8
6
4
2
0
Cre (-)
Wild type
Cre (+)
IC *Nedd4-2*
null
P < 0.05
Wild type
Global
Nedd4-2
null

Figure 5

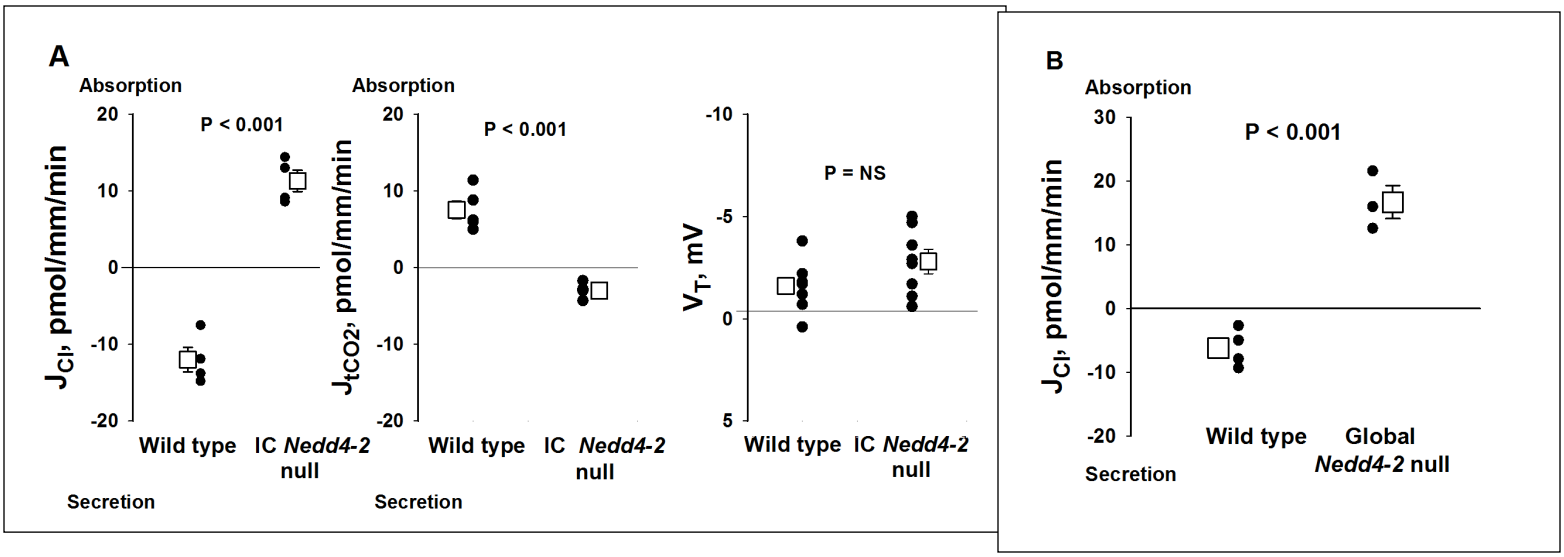
A
Absorption
Secretion
J_{Cl}, pmol/mm/min
20
10
0
-10
-20
P < 0.001
Wild type
IC *Nedd4-2* null
Absorption
Secretion
J_{tCO2}, pmol/mm/min
20
10
0
-10
-20
P < 0.001
Wild type
IC *Nedd4-2* null
V_T, mV
-10
-5
0
5
P = NS
Wild type
IC *Nedd4-2* null
B
Absorption
Secretion
J_{Cl}, pmol/mm/min
30
20
10
0
-10
-20
P < 0.001
Wild type
Global *Nedd4-2* null

Figure 6

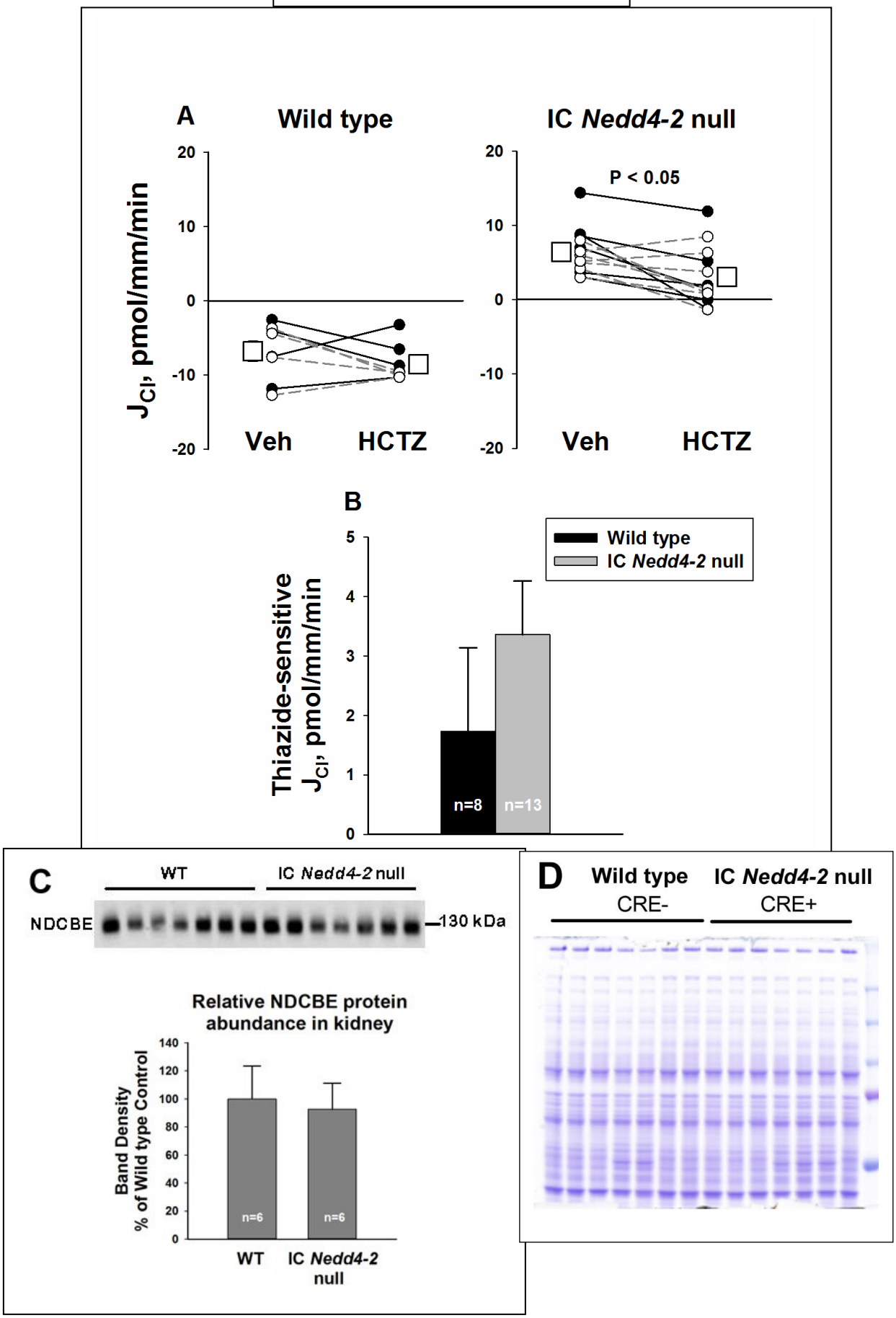
A
Wild type
IC Nedd4-2 null
P < 0.05
J_{Cl}, pmol/mm/min
20
10
0
-10
-20
Veh
HCTZ
B
Wild type
IC Nedd4-2 null
Thiazide-sensitive J_{Cl}, pmol/mm/min
5
4
3
2
1
0
n=8
n=13
C
WT
IC Nedd4-2 null
NDCBE
130 kDa
Relative NDCBE protein abundance in kidney
Band Density % of Wild type Control
140
120
100
80
60
40
20
0
n=6
n=6
WT
IC Nedd4-2 null
D
Wild type
CRE-
IC Nedd4-2 null
CRE+

Figure 7

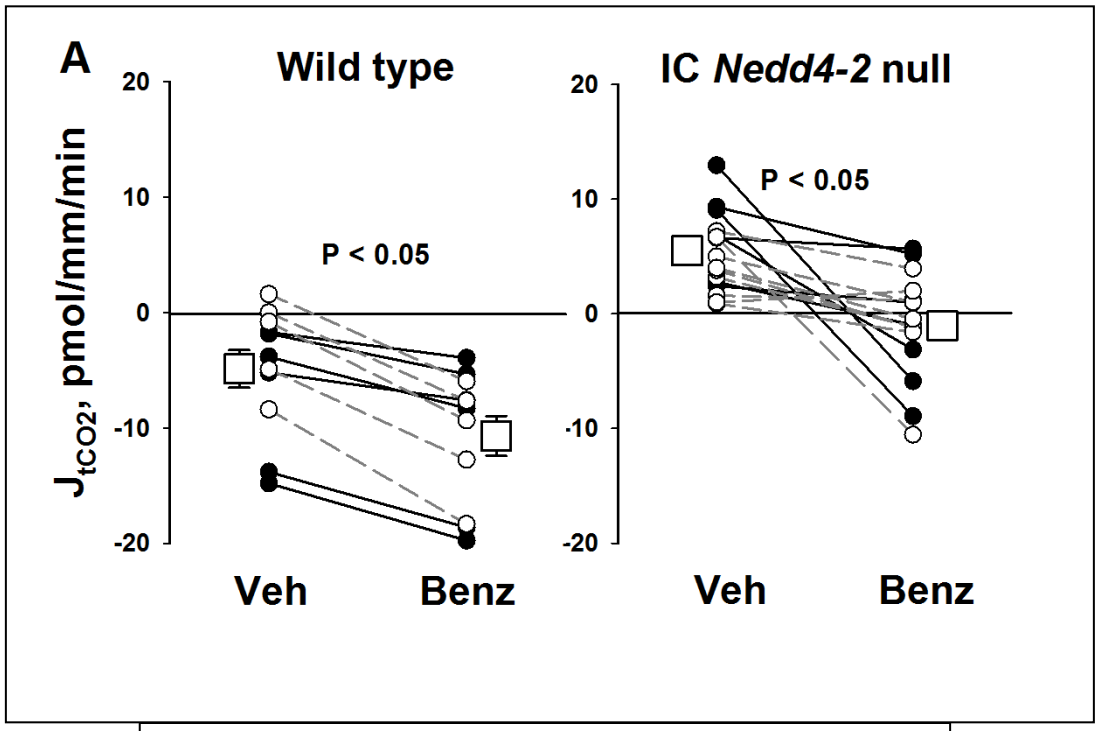
A
Wild type
IC Nedd4-2 null
J_{tCO2}, pmol/mm/min
20
10
0
-10
-20
P < 0.05
P < 0.05
Veh
Benz
Veh
Benz

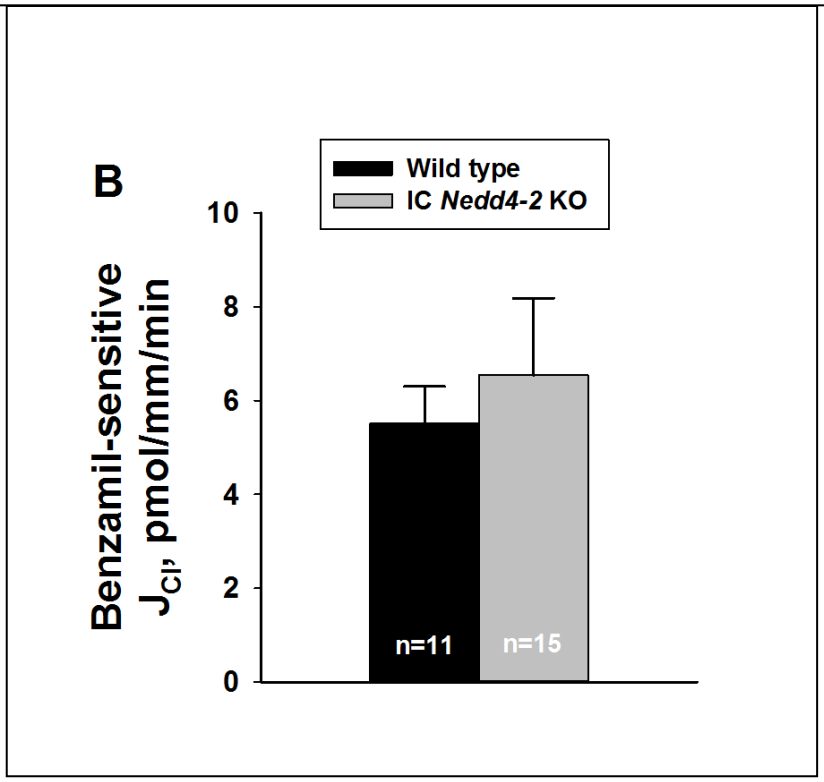
B
Wild type
IC Nedd4-2 KO
Benzamil-sensitive
J_{Cl}, pmol/mm/min
10
8
6
4
2
0
n=11
n=15

Figure 8

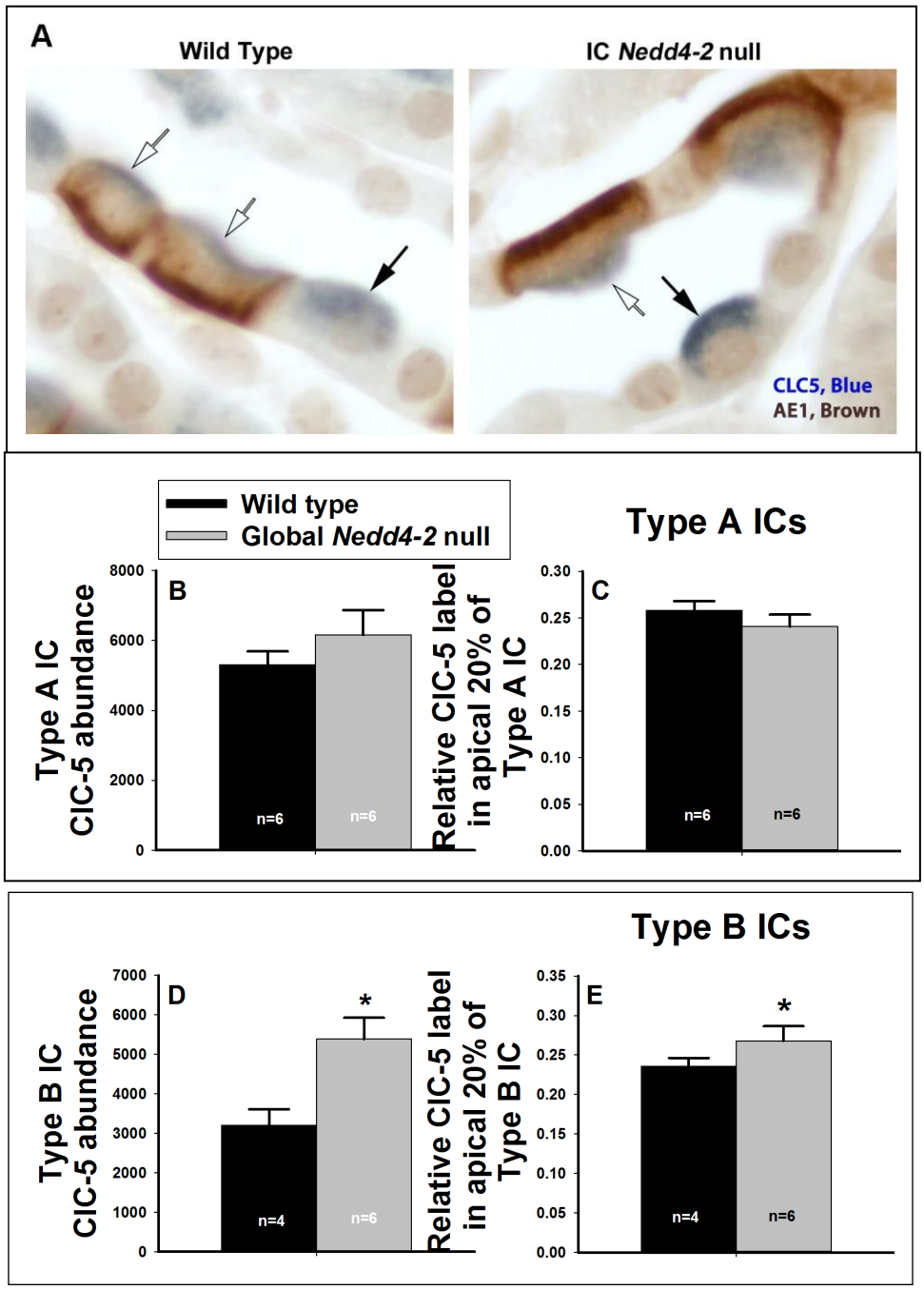
A
Wild Type
IC Nedd4-2 null
CLC5, Blue
AE1, Brown
Wild type
Global Nedd4-2 null
Type A ICs
B
Type A IC
CIC-5 abundance
8000
6000
4000
2000
0
n=6
n=6
C
Relative CIC-5 label
in apical 20% of
Type A IC
0.30
0.25
0.20
0.15
0.10
0.05
0.00
n=6
n=6
Type B ICs
D
Type B IC
CIC-5 abundance
7000
6000
5000
4000
3000
2000
1000
0
*
n=4
n=6
E
Relative CIC-5 label
in apical 20% of
Type B IC
0.35
0.30
0.25
0.20
0.15
0.10
0.05
0.00
*
n=4
n=6

Figure 9

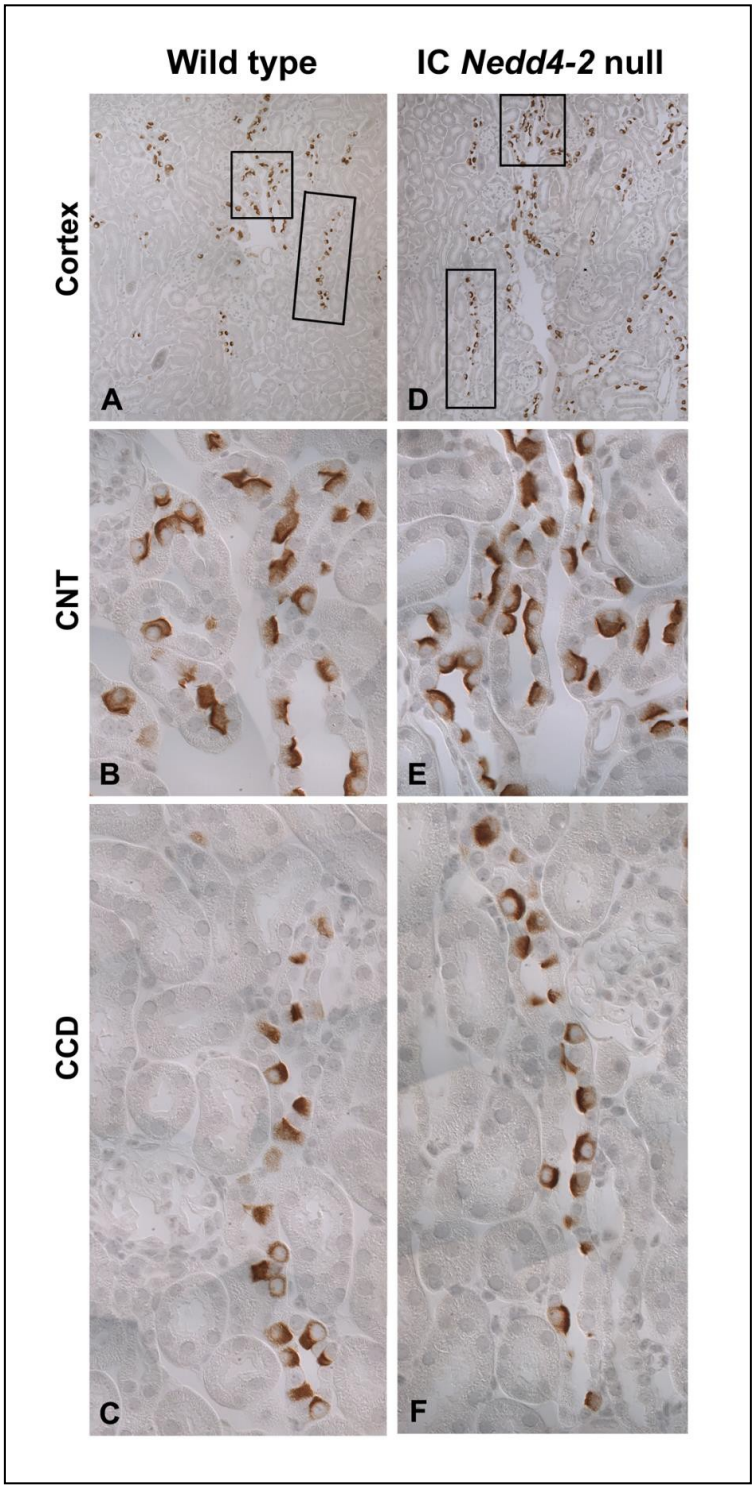

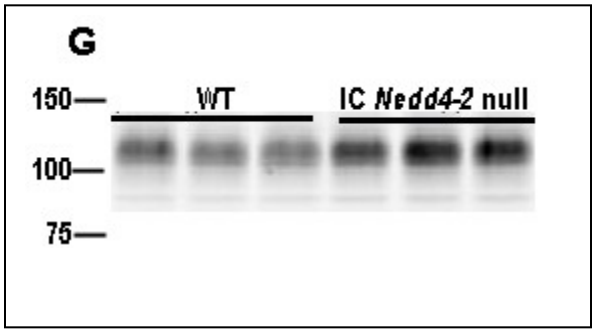
G
150
100
75
WT
IC Nedd4-2 null

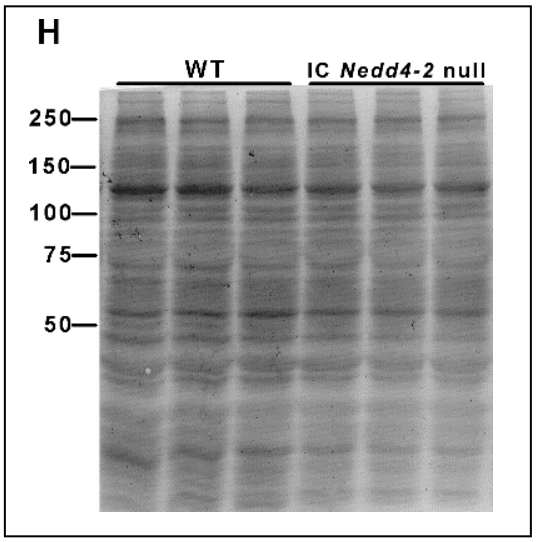
H
WT
IC Nedd4-2 null
250
150
100
75
50

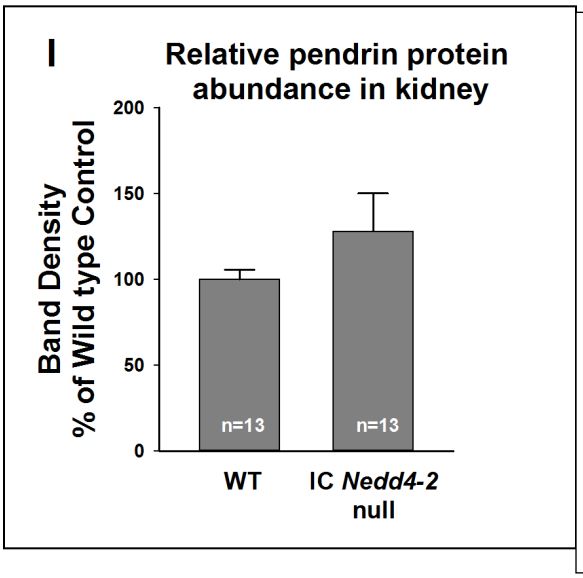
I
Relative pendrin protein abundance in kidney
Band Density
% of Wild type Control
200
150
100
50
0
n=13
n=13
WT
IC Nedd4-2 null

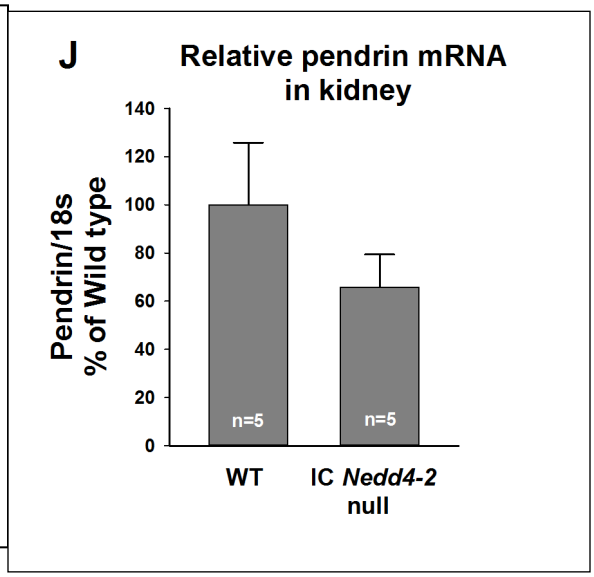
J
Relative pendrin mRNA in kidney
Pendrin/18s
% of Wild type
140
120
100
80
60
40
20
0
n=5
n=5
WT
IC Nedd4-2 null

Figure 10

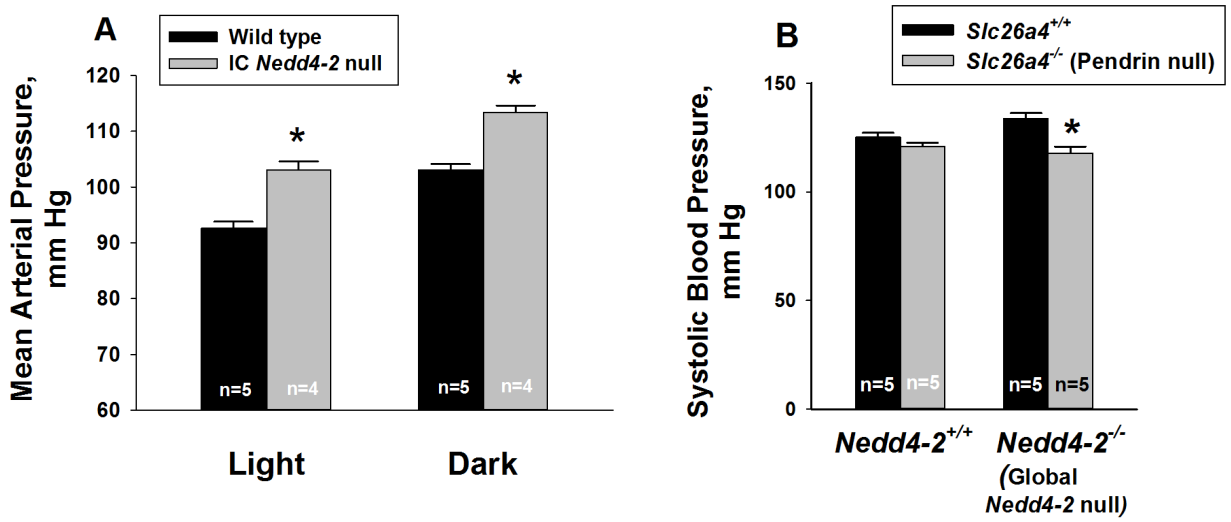
A
Wild type
IC Nedd4-2 null
Mean Arterial Pressure, mm Hg
120
110
100
90
80
70
60
*
*
n=5
n=4
n=5
n=4
Light
Dark
B
Slc26a4+/+
Slc26a4-/- (Pendrin null)
Systolic Blood Pressure, mm Hg
150
100
50
0
*
n=5
n=5
n=5
n=5
Nedd4-2+/+
Nedd4-2-/-
(Global Nedd4-2 null)

SUPPLEMENTAL METHODS

Animals: In all perfused tubule experiments, mice were euthanized by cervical dislocation. In all other experiments, mice were anesthetized with 1-2% isofluorane/100% O_2. The Institutional Animal Care and Use Committee at Emory University approved all treatment protocols.

Measurement of serum aldosterone, arterial blood gases and serum electrolytes: Arterial blood was collected through the abdominal aorta under anesthesia with 1-2% isofluorane in 100% O_2. Serum aldosterone concentration was measured by radioimmunoassay at the Cardiovascular Pharmacology Research Laboratory, University of Iowa College of Pharmacy. Serum electrolytes and arterial blood gases were measured using an iSTAT System (Abbot Point of Care, Princeton, NJ).

In vitro perfusion of isolated CCDs: CCDs were dissected from medullary rays and perfused and bathed at flow rates of 2-3 nl/min in the presence of a symmetric, HCO_3^--buffered physiological solution containing in mM: 125 NaCl, 24 $NaHCO_3$, 2.5 K_2HPO4, 2 $CaCl_2$, 1.2 $MgSO_4$ and 5.5 glucose. Tubules were equilibrated at 37°C for 30 min prior to starting the collections. Stock solutions of benzamil hydrochloride (3 x 10^{-3} M) and bafilomycin (10^{-5} M) were prepared in water and absolute ethanol, respectively. A hydrochlorothiazide stock solution (10^{-1} M) was prepared in DMSO. All chemicals were purchased from Sigma-Aldrich, St. Louis, MO.

Measurement of net transepithelial Cl^- flux. Cl^- concentration was measured in perfusate and collected samples using a continuous-flow fluorimeter and the Cl^- sensitive fluorophore, 6 methoxy-N-(3-sulfopropyl) quinolinium (SPQ; Molecular Probes, Eugene, OR), as described previously (1).

Transepithelial Cl^- flux, J_{Cl}, was calculated according to the equation:

$$J_{Cl} = (C_o - C_L)Q/L$$

where C_o and C_L are perfusate and collected fluid Cl^- concentrations, respectively. Q is flow rate in nl/min. L is tubule length. Net fluid transport was taken to be zero since net fluid flux has not been observed in CCDs when perfused in vitro in the presence of symmetric solutions and in the absence of vasopressin (2, 3).

Measurement of transepithelial HCO_3^- flux, J_{tCO2}: Total CO_2 ($HCO_3^- + H_2CO_3 + CO_2$) concentration, which is mainly HCO_3^- in most physiological solutions, was measured in the perfusate and in collected samples using a continuous-flow fluorimeter with the method of Zhou et al. (4, 5). Transepithelial total CO_2 flux, J_{tCO2}, was calculated as above. Both J_{tCO2} and J_{Cl} were expressed in pmol/mm/min.

Transepithelial voltage (V_T) was measured in the perfusion pipette connected to a high impedance electrometer through an agar bridge saturated with 0.16 M NaCl and a calomel cell as described previously (6). The reference was an agar bridge from the bath to a calomel cell.

***Immunohistochemistry, Imunofluorescence and Quantative Analysis of Immunohistochemistry*:**

For all single and double labeling experiments, we used antibodies to aquaporin 2 (7), *Nedd4-2* (8), pendrin (9), AE1 (Alpha diagnostic International, San Antonio, TX, Catalogue #AE11-A), barttin (10), AE4 (11), and the α4 subunit of the H^+-ATPase (12), all of which have been described previously. The bartin, AE4 and α4-H^+-ATPase antibodies were generous gifts of Drs. Thomas Jentsch, Christian Hubner and Fiona Karet, respectively.

We used Cre reporter mice (dTomato mice, Jackson Labs, #7909) to explore the extent of Cre recombinase expression within the CCD of the intercalated cell *Nedd4-2* null mice. Thus, intercalated

cell *Nedd4-2* null mice were bred with dTomato homozygotes and the resultant offspring studied. To localize Cre recombinase in the intercalated cells, kidneys from these offspring were fixed *in situ* with 4% paraformaldehyde (PFA) in 0.1M phosphate buffer saline (PBS) and post-fixed for 4 hr in 4% PFA at 4°C. Kidneys were cryoprotected in 30% sucrose overnight at 4°C and frozen quickly in optimal cutting temperature (OCT) compound (Tissue-Tek) by immersion in a mixture of dry ice and 2-Methybutane. 5 μm-thick sections were quenched with 50 mM ammonium chloride to reduce autofluorescence and washed in PBS, blocked with Dako serum free ready-to-use protein block (Agilent, Santa Clara, CA) and incubated overnight at 4°C in both anti-pendrin and anti-AE1 antibodies diluted in Dako antibody diluent (Agilent) at 1:3000 and 1:5000, respectively. Sections were then washed and incubated with affinity purified Dylight 488-conjugated goat anti-rabbit IgG antibody (Vector Laboratories, Burlingame, CA) diluted at 1:150 in PBS and incubated for 30 min in dim light at room temperature. Sections were washed, mounted in Prolong Gold antifade (Invitrogen, Carlsbad, CA) and imaged using a Zeiss Axioskop 2 Plus Fluorescence with dual AxioCam HR cameras.

For standard immunohistochemistry, kidneys were fixed *in situ* and embedded in paraffin or polyester wax [polyethylene glycol 400 distearate (Polysciences, Warrington, PA) and 10% 1-hexadecanol] as described previously (13). Immunoreactivity was detected using immunoperoxidase procedures. Blocking was done with 3% H_2O_2 in methanol for 30 minutes, followed by protein blocking using 1% bovine serum albumin, 0.2% gelatin, 0.05% saponin solution. Sections were incubated in the primary antibody diluted in PBS overnight at 4°C. Sections were rinsed with 0.1% BSA, 0.05% saponin and 0.2% gelatin in PBS and incubated with horseradish peroxidase-conjugated goat anti-rabbit secondary antibody (1:200, DAKO) for 2h, washed with PBS and incubated with diaminobenzidine (DAB substrate kit, Vector). Sections were washed in with distilled water, counter stained with hematoxylin, dehydrated with graded ethanols and xylene, mounted and observed by light microscopy.

Double immunolabeling was done using sequential immunoperoxidase procedures as described previously (14). Tissue sections were labeled with the anti-*Nedd4-2* antibody. After the DAB reaction, sections were washed in PBS and blocked again using 3% H_2O_2 in methanol. A second immunolabeling procedure was done on the same sections using the AQP2 as the primary antibody and Vector SG (Vector Laboratories, Burlingame, CA) for the peroxidase substrate, which produces a blue reaction product easily distinguished from the DAB brown reaction product. Sections were then washed with glass distilled water, dehydrated with graded ethanols and xylene, mounted, and observed by light microscopy.

Transporter subcellular distribution was quantified as described previously in bright field light micrographs (15). High-resolution digital micrographs were taken of defined tubule segments using a Leica DM2000 microscope and a Leica DFC425 digital camera (14.4-megapixel images, 63X objective) and Leica DFC Twain Software and LAS application suite (Leica Microsystems, Buffalo Grove, IL). Pixel intensity across a line drawn from the tubule lumen through the center of an individual cell was quantified with NIH ImageJ, version 1.34s software. Background pixel intensity was calculated as the mean pixel intensity outside the cell and was subtracted from the pixel intensity at each point. Total cellular expression was determined by integrating net pixel intensity across the entire cell. Cell height was determined as the distance in pixels between the apical and the basolateral edges of the cell. Immunoreactivity expressed at zones throughout the cell was determined by integrating pixel intensity at this region. The individual performing the microscopy and quantifying the results was blinded as to the treatment group of each animal. Data from all cells in the CCD of a given subtype, i.e. type A and type B intercalated cells, were averaged for each animal and used in the statistical analysis.

***Immunogold cytochemistry with morphometric analysis*:**

Kidneys were prepared for electron microscopy as described previously (16). Pendrin immunoreactivity was localized in ultrathin sections using immunogold cytochemistry (16, 17). Type B and Non-A, non-B intercalated cells in the CCD were identified using morphological characteristics established in studies of the mouse under basal conditions along with the presence of pendrin immunolabel (16). Apical plasma membrane boundary length, cytoplasmic area and gold label touching the apical plasma membrane and gold label in the cytoplasm, including cytoplasmic vesicles were quantified in type B and Non-A, non-B intercalated cells as described previously (16). For each animal, at least 5 cells in each subtype were selected at random and photographed at a primary magnification of X 15,000 and examined at a final magnification of ~ X 36,000. Raw morphometric data from individual cell profiles were pooled to generate an average value for each cell type for each animal. The "n" reported reflects the number of mice studied.

Quantitative PCR

Kidneys were harvested, immediately snap frozen in liquid nitrogen and stored at -80 ^{o}C, and then homogenized in 300uL of TRIzol reagent (Invitrogen, Hopkinton, MA). RNA extraction was performed using the manufacturer's instructions. To remove DNA, samples were then incubated with DNase I (Thermo Scientific, Waltham, MA) and Reaction Buffer with $MgCl_2$ for DNase I (10X) (Thermo Scientific, Waltham, MA) at 37 ^{o}C for 30 min. 1 μl of EDTA was added and the mixture was incubated again at 65 ^{o}C for 10 min.

Reverse transcription was performed using the Thermoscript RT-PCR kit (Invitrogen, Carlsbad, CA). Quantitative PCR was performed using a Bio-Rad cycler (Hercules, CA) with SYBR Green PCR Reagents (Bio-Rad, Hercules, CA). The following cycle parameters were used: 95°C for 1 min and 40 cycles at 95°C for 20 s, 55°C for 30 s, and 72°C for 30 s. The quantification cycle (Cq) values was defined

as the number of cycles required for the fluorescence signal to exceed the detection threshold. Individual mRNA expression was standardized to 18S gene, and expression was calculated as the difference between the threshold values of the two genes (2-ΔΔCq). Melting curve analysis was always performed during qPCR to analyze and verify the specificity of the reaction. With each sample, the assay was performed in triplicate. The results of these triplicate measurements were averaged to get a single value for each mouse that was used in the analysis.

Primers:
mouse Pendrin (NM_011867.3):

F 5' GACTGTAAAGACCCTCTTGATCTGA 3',
R 5' GGAAGCAAGTCTACGCATGG 3';
Amplicon 90

mouse 18S (X00686):
F 5'-CGG CTA CCA CAT CCA AGG AAG G-3',
R 5'-CCC GCT CCC AAG ATC CAA CTA C-3'.
Amplicon 101

Immunoblots:

Immunoblots of kidney lysates were performed using methods reported previously (18, 19). Whole kidney lysates were isolated by harvesting mouse kidneys and placing them in an ice cooled buffer (0.3 M sucrose, 25 mM imidazole, pH 7.2, containing 1x Roche Complete Protease Inhibitor Cocktail). Tissue was immediately homogenized using an Omni THQ Tissue Homogenizer (Omni International) and then centrifuged at 1000 x g for 15 min at 4ºC. To prepare whole cell lysates, intercalated cells were homogenized in Gentle Lysis Buffer (10 mM Tris·HCl, 10 mM NaCl, 2 mM EDTA, 0.5% NP-40, 1% glycerol, and Na_3VO_4 and freshly added 0.18 μg/ml Na_3VO_4, 10 μg/ml PMSF, 5 μg/ml aprotinin, and 1 μg/ml leupeptin). To enable equal protein loading in each lane, protein content in the soluble fraction of

homogenates was measured using a RC-PC protein assay kit (DC Protein Assay Kit, Bio-Rad, Hercules, CA) and then dissolved in Laemmli buffer.

Aliquots containing equal amounts of protein from these lysates were separated by SDS-PAGE on 8.5% acrylamide gels and then electroblotted to PVDF membranes (Immobilon, Millipore, Bedford, MA). Blots were blocked with Odyssey Blocking Buffer (LI-COR Biosciences) following the manufacturer's instructions and then incubated with primary antibody overnight at 4°C, followed by incubation for 2 hours at room temperature with Alexa Fluor 680-linked anti-rabbit IgG (Invitrogen). Pendrin protein was detected by immunoblot using a rabbit anti-rat pendrin antibody described previously (9). To correct for possible differences between lanes in lysate protein loading, membranes were Coomassie stained as reported previously (20). Signals were visualized with an Odyssey Infrared Imaging System (LI-COR Biosciences). Immunoblot and Coomassie band densities were quantified using software program Image J (NIH, available at http://rsb.info.nih.gov/). Pendrin band density was normalized to the density of the Coomassie gel band with the same mobility. To quantify NDCBE renal protein abundance, immunoblots of kidney membrane lysates were performed as described previously (21).

Blood pressure measurements:

Blood pressure was measured in conscious mice by telemetry using methods we have reported previously (18, 22). These measurements were made by an observer that was blinded as to the genotype of each mouse. Systolic blood pressure was also measured in conscious mice by tail cuff using a B-2000 (Visitech Systems), as we reported previously (15). To condition mice for tail cuff blood pressure readings, animals were placed in a platform for 15 min on 2 consecutive days. Over the next 3-4 consecutive days, mice were placed on the platform and at least four readings were taken. All conditioning and all blood pressure readings were performed at the same location under quiet, low-light

conditions. Measurements and conditioning were performed by the same operator at the same time of day.

Statistical Analysis:

For each CCD perfused in vitro, one to two replicate J_{tCO2} or J_{Cl} measurements were made under each condition. The flux reported for each mouse represents the mean of all replicate measurements made under that condition. The "n" reported represents the number of mice studied. Just 1 tubule was studied per mouse. In quantitative immunohistochemistry experiments, for each mouse studied label was quantified in 8-16 cells from each cell subtype. For immunogold studies, gold label was quantified in 5-12 type B intercalated cells and in 5-18 non-A, non-B intercalated cells from each mouse. In each mouse studied, these replicates were averaged to get a single value for each cell type. When comparing two groups, statistical significance was determined using a paired or unpaired two-tailed Student's t test, as appropriate. Data are displayed as the mean ± SEM.

REFERENCES

1. Garcia NH, Plato CF, and Garvin JL. Fluorescent determination of chloride in nanoliter samples. *Kidney Int.* 1999;55(321-5.

2. Knepper MA, Good DW, and Burg MB. Ammonia and bicarbonate transport by rat cortical collecting ducts perfused in vitro. *AmJPhysiol.* 1985;249(F870-F7.

3. Knepper MA, Good DW, and Burg MB. Mechanism of ammonia secretion by cortical collecting ducts of rabbits. *AmJPhysiol.* 1984;247(F729-F38.

4. Pech V, Zheng W, Pham TD, Verlander JW, and Wall SM. Angiotensin II activates H+-ATPase in type A intercalated cells in mouse cortical collecting duct. *JAmSocNephrol.* 2008;19(84-91.

5. Zhou Y, Bouyer P, and Boron WF. Role of tyrosine kinase in the CO_2-induced stimulation of HCO_3^- reabsorption by rabbit S2 proximal tubules. *AmJPhysiol.* 2006;291(F358-F67.

6. Wall SM. NH_4^+ augments net acid secretion by a ouabain-sensitive mechanism in isolated perfused inner medullary collecting ducts. *AmJPhysiol.* 1996;270(F432-F9.

7. DiGiovanni SR, Nielsen S, Christensen EI, and Knepper MA. Regulation of collecting duct water channel expression by vasopressin in Brattleboro rat. *ProcNatlAcadSciUSA.* 1994;91(8984-8.

8. Flores SY, Loffing-Cueni D, Kamynina E, Daidie D, Gerbex C, Chabanel S, Dudler J, Loffing J, and Staub O. Aldosterone-induced serum and glucocorticoid-induced kinase 1 expression is accompanied by Nedd4-2 phosphorylation and increased Na+ transport in cortical collecting duct cells. *JAmSocNephrol.* 2005;16(2279-87.

9. Knauf F, Yang C-L, Thomson RB, Mentone SA, Giebisch G, and Aronson PS. Identification of a chloride-formate exchanger expressed on the brush border membrane of renal proximal tubule cells. *ProcNatlAcadSciUSA.* 2001;98(9425-30.

10. Estevez R, Boettger T, Stein V, Birkenhager R, Otto E, Hildebrandt F, and Jentsch TJ. Barttin is a Cl^- channel β subunit-crucial for renal Cl- reabsorption and inner ear K^+ secretion. *Nature.* 2001;414(558-61.

11. Chambrey R, Kurth I, Peti-Peterdi J, Houillier P, Purkerson JM, Leviel F, Hentschke M, Zdebik AA, Schwartz GJ, Hubner CA, et al. Renal intercalated cells are rather energized by a proton than a sodium pump. *Proc Natl Acad Sci U S A.* 2013;110(19):7928-33.

12. Dou H, Xu J, Wang Z, Smith AN, Soleimani M, Karet FE, Greinwald JH, and Choo D. Co-expression of pendrin, vacuolar H+-ATPase a4-subunit and carbonic anhydrase II in epithelial cells of the murine endolymphatic sac. *JHistochemCytochem.* 2004;52(1377-84.

13. Kim Y-H, Pham TD, Zheng W, Hong S, Baylis C, Pech V, Beierwaltes WH, Farley DB, Braverman LE, Verlander JW, et al. Role of pendrin in iodide balance: going with the flow. *AmJPhysiol.* 2009;297(1069-79.

14. Kim Y-H, Verlander JW, Matthews SW, Kurtz I, Shin WK, Weiner ID, Everett LA, Green ED, Nielsen S, and Wall SM. Intercalated cell H+/OH- transporter expression is reduced in *Slc26a4* null mice. *AmJPhysiol.* 2005;289(F1262-F72.

15. Verlander JW, Hong S, Pech V, Bailey JL, Agazatian D, Matthews SW, Coffman TM, Le T, Inagami T, Whitehill FM, et al. Angiotensin II acts through the angiotensin 1a receptor to upregulate pendrin. *AmJPhysiol.* 2011;301(F1314-F25.

16. Wall SM, Hassell KA, Royaux IE, Green ED, Chang JY, Shipley GL, and Verlander JW. Localization of pendrin in mouse kidney. *AmJPhysiol.* 2003;284(F229-F41.

17. Verlander JW, Hassell KA, Royaux IE, Glapion DM, Wang ME, Everett LA, Green ED, and Wall SM. Deoxycorticosterone upregulates PDS (Slc26a4) in mouse kidney: role of pendrin in mineralocorticoid-induced hypertension. *Hypertension.* 2003;42(3):356-62.

18. Kim Y-H, Pech V, Spencer KB, Beierwaltes WH, Everett LA, Green ED, Shin WK, Verlander JW, Sutliff RL, and Wall SM. Reduced ENaC expression contributes to the lower blood pressure observed in pendrin null mice. *AmJPhysiol.* 2007;293(F1314-F24.

19. Klein JD, Martin CF, Kent KJ, and Sands JM. Protein kinase C-alpha mediates hypertonicity-stimulated increase in urea transporter phosphorylation in the inner medullary collecting duct. *Am J Physiol Renal Physiol.* 2012;302(9):F1098-103.

20. Welinder C, and Ekblad L. Coomassie staining as loading control in western blot analysis. *JProteome Res.* 2011;10(1416-9.

21. Sinning A, Radionov N, Trepiccione F, Lopez-Cayuqueo KI, Jayat M, Baron S, Corniere N, Alexander RT, Hadchouel J, Eladari D, et al. Double Knockout of the Na+-Driven Cl-/HCO3- Exchanger and Na+/Cl- Cotransporter Induces Hypokalemia and Volume Depletion. *J Am Soc Nephrol.* 2017;28(1):130-9.

22. Pech V, Pham TD, Hong S, Weinstein AM, Spencer KB, Duke BJ, Walp E, Kim Y-H, Sutliff RL, Bao H-F, et al. Pendrin modulates ENaC function by changing luminal HCO_3^-. *JAmSocNephrol.* 2010;21(1928-41.

SUPPLEMENTAL DATA

Supplemental Table 1: Effect of IC *Nedd4-2* gene ablation on H^+-ATPase abundance and subcellular distribution in mouse CCD				
	Type A Intercalated Cells		Type B Intercalated Cells	
	Cre (-), floxed *Nedd4-2*, Wild type littermates	IC *Nedd4-2* null	Wild type	IC *Nedd4-2* null
Cell height, arbitrary units	1.63 ± 0.13	1.55 ± 0.05	1.55 ± 0.1	1.54 ± 0.05
Total cell expression (pixel intensity), arbitrary units, X 10^{-1}	1018 ± 125	944 ± 16	734 ± 101	748 ± 52
Apical expression ratio (expression in the apical 20% relative to total expression)	0.218 ± 0.016	0.209 ± 0.005	NA	NA
Basolateral expression ratio (expression in the basolateral 25% relative to total expression)	NA	NA	0.225 ± 0.011	0.214 ± 0.011
Values were determined using quantitative immunohistochemistry; N=5 mice in each group; NA, not applicable, P = NS. Mice consumed the NaCl-rich diet (1.4 meq/d NaCl) for 7 days before sacrifice.				

SUPPLEMENTAL FIGURES

Supplemental Figure 1: Intercalated cell *Nedd4-2* gene ablation produces little change in CCD H^+ secretion and no detectable change in apical H^+-ATPase immunolabel. Panel A: J_{tCO2} was measured in CCDs from IC *Nedd4-2* knockout (n=5) and wild type littermates (n=5) with either bafilomycin (5 nM) or vehicle in the perfusate. Solid lines indicate experiments in which vehicle was present in the first period and bafilomycin added in the second. The dashed lines show the reverse order, i.e. bafilomycin present in period one and then removed in period two. The right panel shows that the bafilomycin-sensitive component of $JtCO_2$ was low and not significantly different between groups.

Panel B shows a representative cortical collecting duct from an IC *Nedd4-2* null and a wild type littermate labeled for the α4 subunit of the H^+-ATPase. Arrowheads show H^+-ATPase immunolabel in the apical region of the cell, indicating type A intercalated cells. Arrows show H^+-ATPase immunolabel in the basolateral regions, indicating type B intercalated cells. Although H^+-ATPase expression varied among individual type A and type B intercalated cells, overall *Nedd4-2* gene ablation did not increase label intensity nor did it increase the relative label in the apical or the basolateral plasma membrane region of either intercalated cell subtype.

Supplemental Figure 2: IC *Nedd4-2* gene ablation increases pendrin immunogold label on the apical plasma membrane relative to the cytoplasm in type B intercalated cells of the CCD. The top panel shows gold (pendrin) label in representative type B intercalated cells taken from an IC *Nedd4-2* KO and a wild type littermate. The arrows indicate gold (pendrin) label on the apical plasma membrane,

whereas arrowheads indicate label in the subapical space. The insets mark regions of each micrograph shown at higher magnification in the lower panels.

Supplemental Figure 3: IC *Nedd4-2* gene ablation does not increase barttin label intensity per cell or increase label intensity in the basolateral membrane region. This figure shows barttin label (brown) in cortical sections from IC *Nedd4-2* null and wild type littermates. Sections were double labeled for pendrin (blue) to indicate type B and Non-A, non-B intercalated cells. The upper panels show pendrin and barttin label in cortical sections at low magnification. The regions circumscribed within a box indicate cortical collecting ducts shown at higher magnification in the lower panels. Arrows indicate pendrin-positive, type B intercalated cells, whereas arrowheads indicate pendrin-negative type A intercalated cells. As shown, there was no striking increase in intercalated cell bartin label intensity in the CCDs from IC *Nedd4-2* null relative to their wild type littermates.

Supplemental Figure 4: IC *Nedd4-2* gene ablation does not increase AE4 immunolabel. The upper panel shows sections from an IC *Nedd4-2* null and a wild type littermate that were labeled for AE4. The lower panel shows sections from each group at higher power that were labeled for both AE4 (brown) and for pendrin (blue). As shown, AE4 label intensity is more striking in pendrin positive (arrows) than in pendrin negative cells (arrowheads), which indicates greater expression in either type B or Non-A, non-B (arrows) than in type A intercalated cells (arrowheads). No AE4 label was detected in principal cells. IC *Nedd4-2* gene ablation did not increase AE4 label intensity nor did it increase the relative AE4 label in the region of the plasma membrane.

Supplemental Figure 5: Effect of NaCl intake on systolic blood pressure in IC *Nedd4-2* null and wild type mice. This figure shows systolic blood pressure measured by tailcuff in 6 IC *Nedd4-2* null and 6 wild type littermates following a standard 1% NaCl diet consumed at libitum. Blood pressure was then re-measured in these mice after 14 days of a 4% NaCl diet.

Supplemental Figure 1

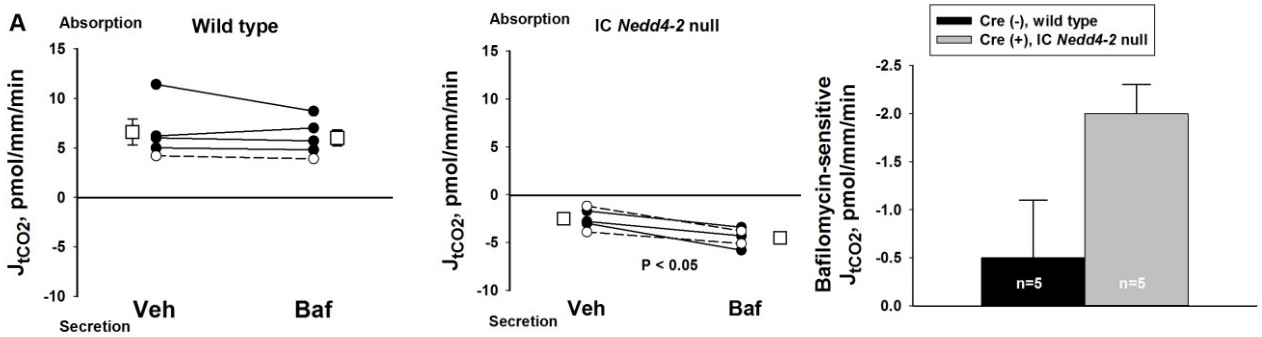

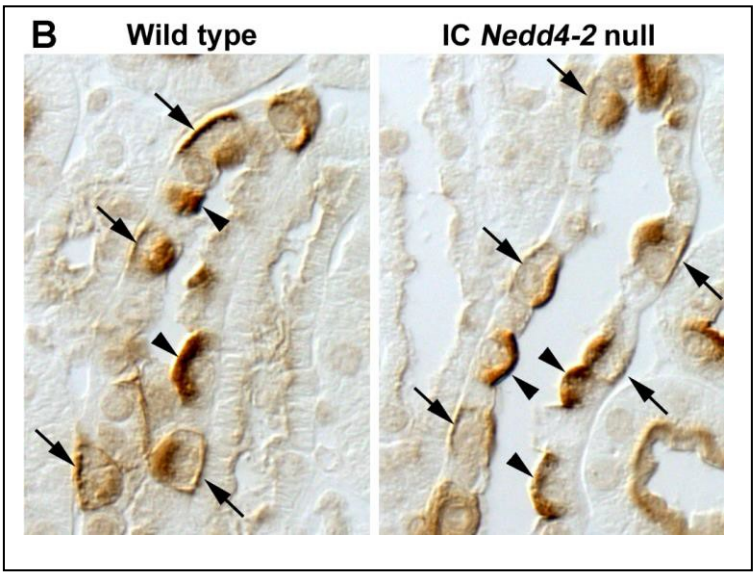

Supplemental Figure 2

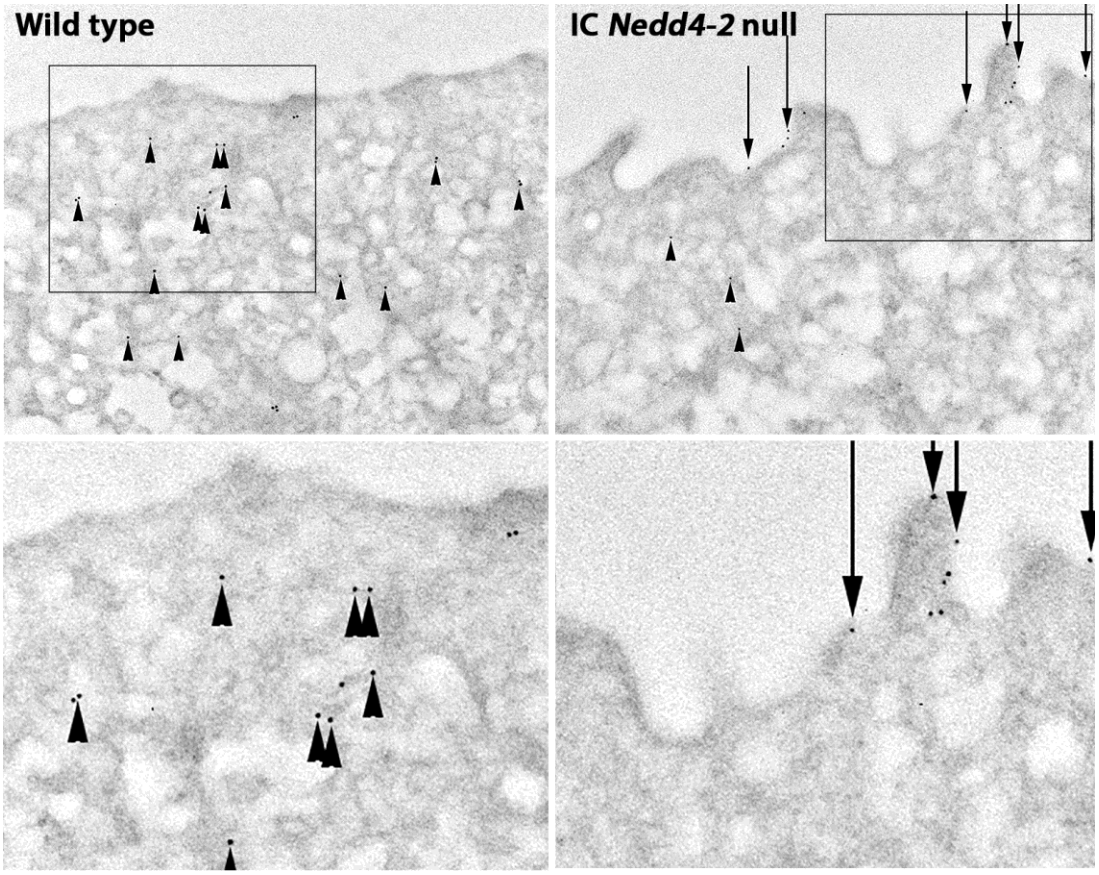

Supplemental Figure 3

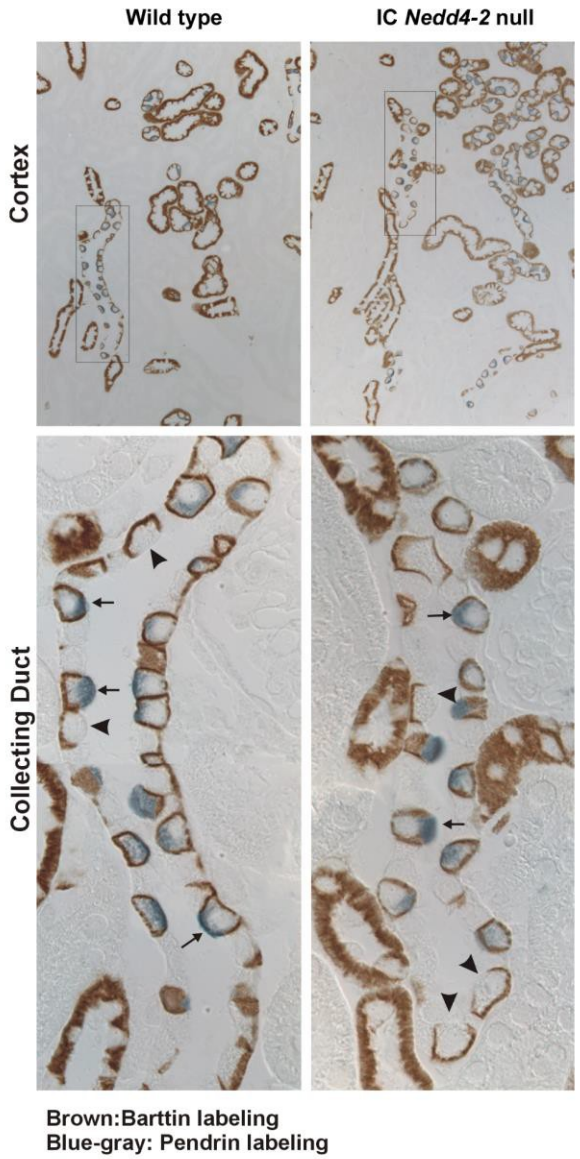

Supplemental Figure 4

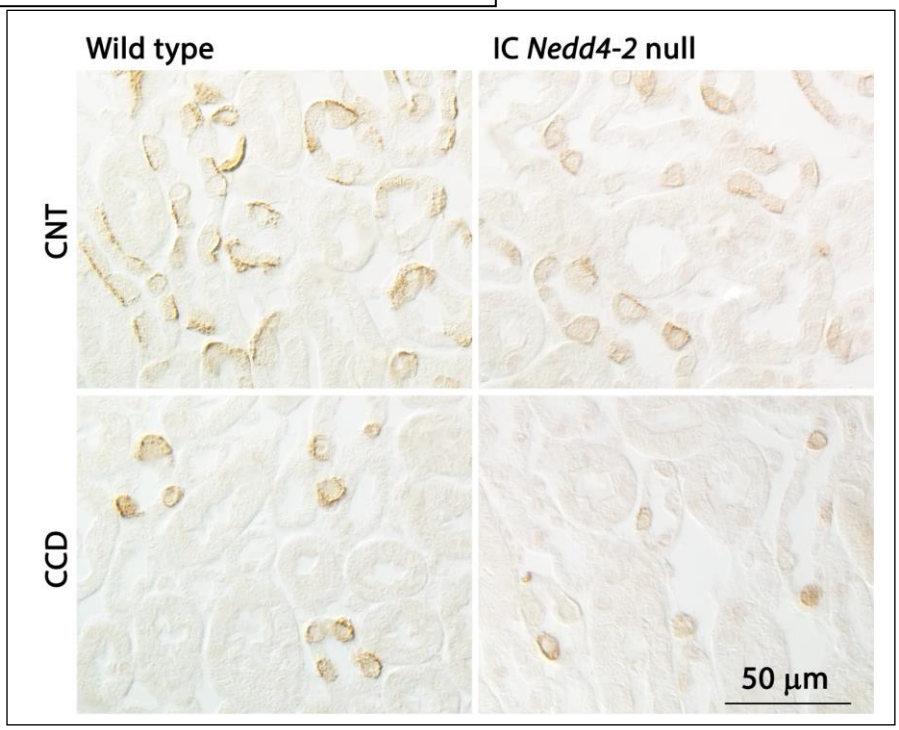

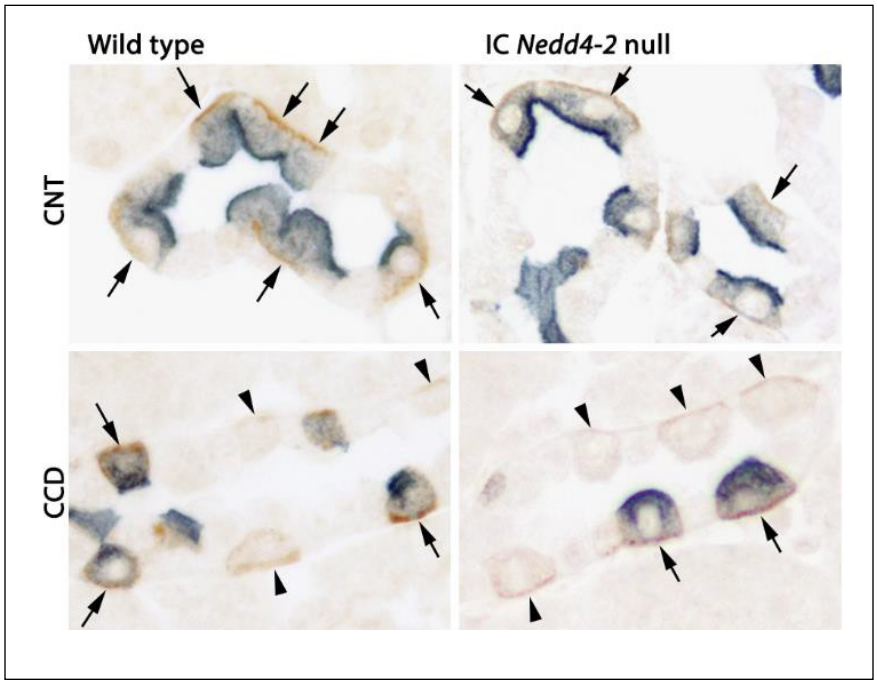

Supplemental Figure 5